NUCLEAR STRUCTURE -- THEORY

A NEW SKYRME INTERACTION FOR NORMAL AND EXOTIC NUCLEI

B. Alex Brown

Since the introduction of the Skyrme interaction by Vautherin and Brink [1], this parameterization has proven remarkably useful and successful for Hartree–Fock (HF) shell–model calculations. It appears to incorporate the essential physics in terms of a minimal parameterization, e.g., an s– and p–wave expansion of an effective nucleon–nucleon interaction together with a density dependent part which accounts for the truncation of the shell–model space to a closed–shell configuration. Since the interaction its phenomenological, the parameters need to be determined from experimental data. It is apparent that the many parameterizations which exist in the literature are quite good. But generally when they are applied to the most exotic neutron–rich and neutron–deficient nuclei which have been experimentally investigated in the last decade, their agreement becomes significantly worse. As an example, the HFB calculations presented in [2] give a binding energy of 832.45 MeV for ^{100}Sn compared to its recently experimental value of 825.8(9) MeV [3]; this size of deviation is typical for all existing Skyrme parameterization, although some are better than others.

It is natural to ask whether or not there is enough flexibility within the Skyrme model to improve the agreement for exotic nuclei. In this work I will show that the agreement for exotic nuclei can be improved dramatically with a relatively small change from the previously known parameters. One of the shortcomings of the conventional Skyrme parameterization is in reproducing the difference in the binding energy of the mirror pairs of nuclei, for example, the difference between ^{48}Ni and ^{48}Ca. This problem is related to the well–known Nolen–Schiffer anomaly for the mirror nuclei with T=1/2 [4]. I find that the displacement energy anomaly can be taken into account in a practical way by allowing the masses which appear in the kinetic energy operator to vary slightly from the bare values.

The first Skyrme parameterizations were obtained from a fit to the properties of ^{16}O, ^{40}Ca, ^{48}Ca, ^{90}Zr, ^{116}Sn and ^{208}Pb. However, with the accumulation of experimental data, these "closed–shell" nuclei are no longer the optimal candidates. It is known that core–excited admixtures may be important for ^{16}O and ^{40}Ca from, for example, the relatively large rms radius of ^{40}Ca [5], the data from nucleon pickup reactions [5, 6] and from large–basis shell–model calculations which allow for core breaking [7, 8]. The nuclei ^{90}Zr and ^{120}Sn may have significant pairing correlations (many of the HF calculations also include these pairing correlations). And finally, the above set of nuclei tend to lie along the valley of stability.

The nuclei considered in this work are ^{16}O, ^{34}Si, ^{40}Ca, ^{48}Ca, ^{48}Ni, ^{88}Sr, ^{100}Sn, ^{132}Sn and ^{208}Pb. All of these have precisely measured binding energies [10], except for ^{48}Ni whose binding energy can be extrapolated to within about 100 keV based upon displacement energy systematics [9] [this data is treated in terms of the mirror binding energy difference BE(^{48}Ca) – BE(^{48}Ni) = 67.06(10) MeV] and for the recently measured ^{100}Sn value cited above. We give the most weight (0.3 MeV in the fit) to ^{34}Si (Ex=3.3 MeV), ^{48}Ca (Ex=3.8 MeV), ^{48}Ni, ^{132}Sn (Ex=4.0 MeV) and ^{208}Pb (Ex=2.6 MeV). All of these have high first excited states [17] (indicated in the brackets). The others are also included but with a lesser weight (1.0 MeV). The pairing correlations for ^{88}Sr (Ex=1.8 MeV) may be important as indicated by its relatively low–lying 2^+ state, and the experimental error for ^{100}Sn is large. In addition the fit includes the rms charge radii [11] ^{16}O (2.737 fm), ^{40}Ca (3.477 fm), ^{48}Ca (3.474 fm), ^{88}Sr (4.219 fm) and ^{208}Pb (5.501 fm) with weights of 0.03 fm for the first two and 0.01 fm for the last three. Of the previous Skyrme parameterizations, perhaps the SKT6 interaction of Tondeur et al. [12] is closest in spirit to the present work. They do consider the

exotic nucleus ^{132}Sn, however, they do not consider ^{48}Ni or ^{100}Sn and they have not taken into account the Nolen-Schiffer anomaly. (In addition, their small α value leads to an rms charge radius for ^{48}Ca which is significantly larger than experiment.)

Also 66 single–particle energies (SPE) are included in the fit; the ones given most weight (0.5 MeV) are 10 which can be obtained for ^{132}Sn (the $2p_{1/2}$, $1g_{9/2}$, $1g_{7/2}$, $2d_{5/2}$ and $2d_{3/2}$ protons and the $1h_{11/2}$, $3s_{1/2}$, $1h_{11/2}$, $2d_{3/2}$ and $2f_{7/2}$ neutrons) and 14 for ^{208}Pb (the $2d_{5/2}$, $1h_{11/2}$, $2d_{3/2}$, $2s_{1/2}$, $1h_{9/2}$, $2f_{7/2}$ and $1i_{13/2}$ protons and the $1i_{13/2}$, $2p_{3/2}$, $2f_{5/2}$, $3p_{1/2}$, $2g_{9/2}$, $1i_{11/2}$ and $1j_{15/2}$ neutrons.) All of these SPE are obtained from the binding energy difference between the appropriate state (ground state or excited state) in the odd–even nuclei and the ground state of the doubly closed–shell nucleus; the data are taken from [10, 17]. It is possible that any given single–particle state may be fragmented due to coupling with low–lying excited states of the core nuclei. We believe that these effects are small for the single–particle states listed above which all lie close to the Fermi surface. Other single–particle states included in the fit are those for the deep hole states of ^{208}Pb [13] and those for lighter nuclei. In both cases fragmentation is more of a problem; and hence they were entered with larger weights, 1.0 MeV for most cases and 2.0 MeV for the SPE in ^{16}O and ^{40}Ca (see below).

For the initial iterations in the least squares fit I started with some existing Skyrme interactions, mainly those of SIII [14], SGII [16], and SKE [15], which have powers of the density dependence of α=1, 1/6 and 0.8, respectively. For a fixed α value the parameters t_0, t_1, t_2, t_3, x_0, x_3 and w_0 are varied. As in [14] and [15] we set x_1 and x_2 equal to zero, since their values are poorly determined by the data set we consider. The center–of–mass correction to the kinetic energy, the spin–orbit potential and the exchange correction to the Coulomb potential are treated the same as in [1, 14]. The rms radii are obtained by folding the point nucleon distributions with the proton and neutron charge distributions [5] and include the spin–orbit correction [5, 15]. Based upon [18, 19, 20], I initially allowed for some mass and N–Z dependence in the spin–orbit interaction, but in the end found that there was little empirical need for these extra terms for the above data set. There is some dependence of the χ^2 on α with a minimum obtained at about α=0.8, which is similar to that of SKE [15]; a small α value of 0.30 gives a χ^2 a factor of two larger. $\{\chi^2 = \sum_i (d_i^{exp} - d_i^{th})^2/[\sigma_i^2(N_d - N_p)]$ where the sum runs over the i data points d_i, σ_i is the weight, N_d is the number of data and N_p are the number of parameters.$\}$

With the above data set and assumptions, the largest contribution to the χ^2 is for the ^{48}Ca – ^{48}Ni binding energy difference which is consistently too small compared to experiment by about 2.5 MeV. This is the same direction as the Nolen–Schiffer anomaly [4], but it is magnified by the large $N - Z$ difference. Unless this is taken into account, there will be a problem with all HF calculations across the $N = Z$ line. Perhaps one could and should introduce a charge–asymmetric strong interaction to account for the Nolen–Schiffer anomaly. However, I find that it can be accounted for equally well by a 1.6 percent increase in the isovector mass, m_1, (the neutron mass minus proton mass) which appears in the kinetic energy. It is not clear that there is any deep justification for doing this, but at least it gives a practical way of taking into account the displacement–energy problem. (The isoscalar mass is kept at its free–nucleon value.)

With the above set of nine parameters (t_0, t_1, t_2, t_3, x_0, x_3, w_0, α, and m_1) a remarkably good fit with $\chi^2 \approx 1.0$ is obtained for the 80 data; this interaction will be denoted by SKX. In particular, the rms deviation for the binding energy of the "best" closed–shell nuclei, ^{34}Si, ^{48}Ca, ^{48}Ni, ^{132}Sn and ^{208}Pb is only 200 keV. The (fitted, experimental) binding energies (in units of MeV) for the other cases is ^{16}O (126.75, 127.62), ^{40}Ca (341.01, 342.05), ^{88}Sr (767.34, 768.47) and ^{100}Sn [824.00, 825.8(9)]; all of these are in the

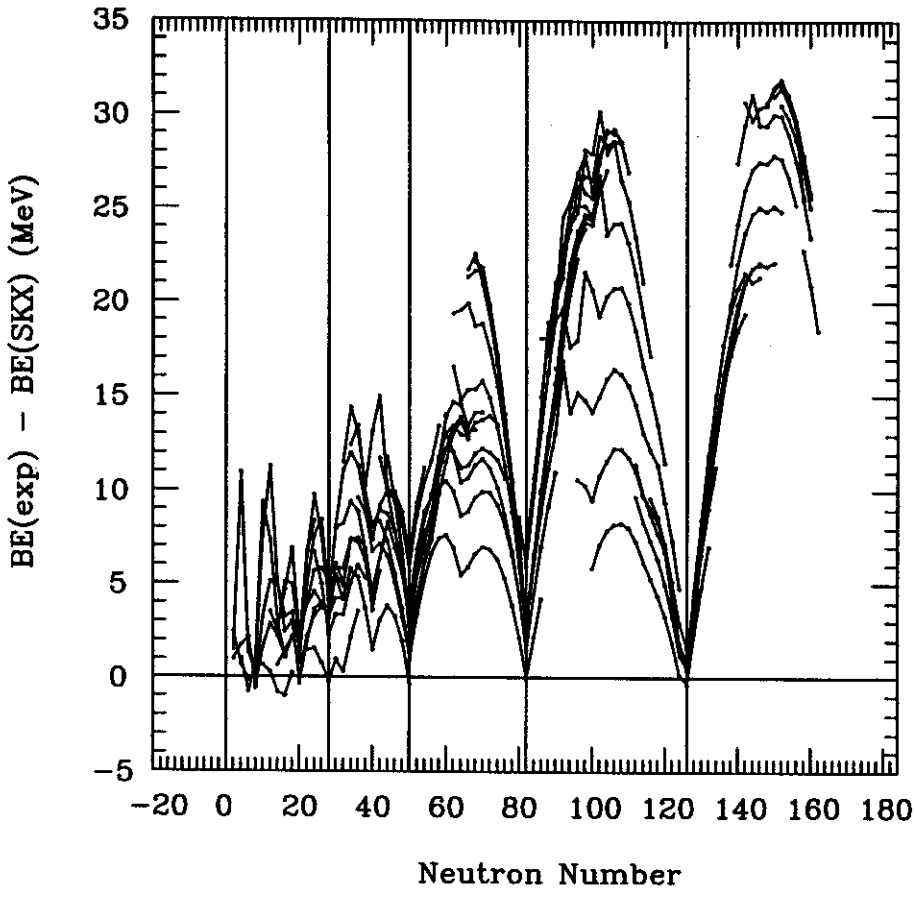

Figure 1: The experimental binding energy minus the calculated value for even-even nuclei. The experimental data includes the extrapolated values of Audi and Wapstra [10]. The data are plotted vs neutron number with those for a given Z value connected by a line. The vertical lines are for the magic numbers 28, 50, 82 and 126.

direction of being theoretically underbound indicating some remaining correlation energy (relative to the "best" doubly–closed shell nuclei). The rms deviations for SPE in ^{132}Sn and ^{208}Pb were both about 400 keV.

The results of using this new Skyrme interaction for the binding energy of all even–even nuclei whose mass is measured experimentally or whose mass is given by the Audi–Wapstra extrapolation [10] (739 nuclei) are shown in Fig. 1. The nucleons are assumed to occupy the lowest available spherical orbital. The comparison is remarkably consistent with all nuclei away from those "best" closed–shell nuclei showing an enhancement in the binding energy due to the pairing and deformation correlations. The other nuclei near zero in Fig. 1 are the mirror pairs ^{14}O (Ex=5.17 MeV) – ^{14}C (Ex=6.09 MeV) and ^{22}O (Ex=3.38 MeV) – ^{22}Si (Ex=3.38 MeV) as well as ^{24}O (Ex=4.18 MeV), where the excitation energies of the first excited states in parentheses are from experiment for $A = 14$ [17] and from sd–shell theory for $A = 22$ and 24 [22]. All of these are candidates for the list of "best" doubly–closed shell nuclei, but they were not included in the fit because I did not want to over emphasize the role of light nuclei. Indeed, if any nucleus is found whose binding energy is significantly smaller than what we calculate, it would be a failure of the parameterization. The major shell effects which appear in Fig. 1 come both from the experimental data and from the calculations. The minor shell effects, as well as the occasional spikes above $N = 28$ which appear in Fig. 1, are primarily due to the very simple integer values of the occupations by which the single–particle states are filled; and this effect will be smoothed out when pairing correlations are put

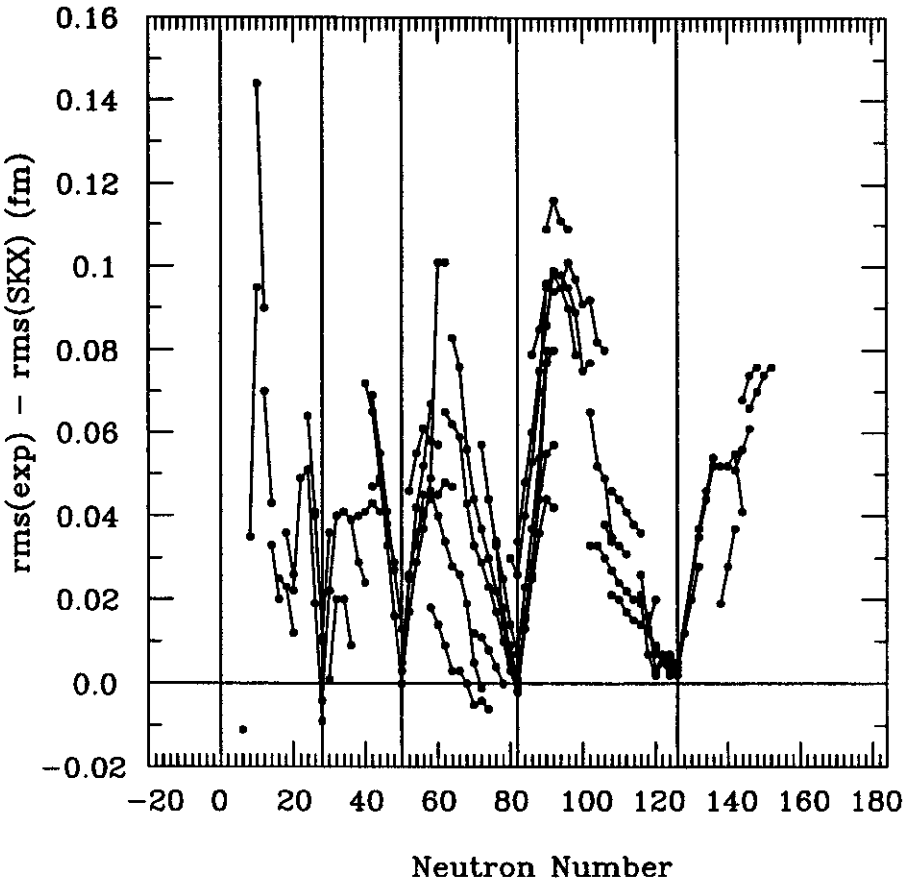

Figure 2: The experimental rms charge radii [11, 21] minus the calculated value for even-even nuclei. The data are plotted vs neutron number with those for a given Z value connected by a line. The vertical lines are for the magic numbers 28, 50, 82 and 126.

into the calculation.

The results for most of the measured charge rms radii [11, 21] are shown in Fig. 2. Again one observes that the "best" closed–shell nuclei are in excellent agreement with the calculations – with those away from the closed shells showing an increase in the rms charge radii due to the vibrational and deformation correlations [23]. In particular, the largest deviation in Fig. 2 is for ^{20}Ne and this is in good agreement with the value of 0.16 fm deduced from its $0^+ \rightarrow 2^+$ B(E2) (see Fig. 4 of [23]). For the most deformed heavy nuclei the largest β_2 correction is 0.12 fm in agreement with the peak around $N = 90$ in Fig. 2. The experimental rms radii for ^{16}O and ^{40}Ca are 0.035 fm and 0.023 fm, respectively, larger than the HF values, again indicating the nonclosed shell aspects of these nuclei. The present interaction gives reasonable agreement with experiment for the interior charge density of ^{208}Pb [11, 13]. There is essentially perfect agreement for $r < 2$ fm with theory being about 3% too low compared to experiment in the region from $2 < r < 5$ fm and with a compensating region being a little too high for $r > 5$ fm. As discussed in [13], this small disagreement in the detail of the ^{208}Pb charge distribution may be due to the p–wave truncation of the nucleon–nucleon interaction which is inherent in the the Skyrme ansatz, or due to non–closed shell (higher–order) contributions to the charge density which cannot be fully taken into account by the simple density–dependent interaction.

The SKX interaction or an extension of it gives the promise of allowing one to carry out HF

calculations for the doubly–closed shell nuclei at an accuracy which matches that of the configuration–mixed shell–model calculations for light nuclei [22], e.g. at the level of a few hundred keV for the binding energy. One is now in a better position to combine the best aspects of both HF and configuration–mixing models. The next step would start with the single–particle results of SKX and add the correlation energy due to the valence interactions, which includes the deformation driving proton–neutron interaction and the like–nucleon interactions (mainly pairing). At the most microscopic level this could be done using the large–basis shell–model methods for light nuclei [22] which are being extended to heavy nuclei with the Monte–Carlo methods [29, 30]. Well–deformed heavy nuclei are probably best treated by the deformed HF methods [31]. In addition, one might use the interaction–boson model for heavy nuclei [32], or at a more qualitative level, the N_p–N_n model [33] may be useful in parameterizing the dependence of the correlation energy between the closed shells and the number of valence protons and neutrons.

References

1. D. Vautherin and D. M. Brink, Phys. Rev. C 5, 626 (1972).
2. J. Dobaczewski, H. Flocard and J. Treiner, Nucl. Phys. A422, 103 (1984).
3. M. Chartier et al., Phys. Rev. Lett. 77, 2400 (1996).
4. J. A. Nolen and J.P. Schiffer, Ann. Rev. Nucl. Sci. 19, 471 (1969).
5. B. A. Brown, S. E. Massen and P. E. Hodgson, Phys. Lett. 85B, 167 (1979); J. Phys. G 5, 1655 (1979).
6. P. Doll, G. J. Wagner, K. T. Knopfle and G. Mairle, Nucl. Phys. A163, 210 (1976).
7. E. K. Warburton, B. A. Brown and D. J. Millener, Phys. Lett. B293, 7 (1992).
8. M. Sakakura, A. Arima and T. Sebe, Phys. Lett. 61B, 335 (1976).
9. B. A. Brown, Phys. Rev. C 43, R1513 (1991).
10. G. Audi and A. H. Wapstra, Nucl. Phys. A595, 409 (1995).
11. G. Fricke, C. Bernhardt, K. Heilig, L. A. Schaller, L. Schellenberg, E. B. Shera and C. W. de Jager, At. Data Nucl. Data Tables, 60, 177 (1995).
12. F. Tondeur, M. Brack, M. Farine and J. M. Pearson, Nucl. Phys. A420, 297 (1984).
13. B. A. Brown, S. E. Massen, J. I. Escudero, P. E. Hodgson and J. Vinas, J. Phys. G 9, 423 (1983).
14. M. Beiner, H. Flocard, N. van Giai and P. Quentin, Nucl. Phys. A238, 29 (1975).
15. J. Friedrich and P.-G. Reinhard, Phys. Rev. C 33, 335 (1986).
16. N. van Giai and H. Sagawa, Nucl. Phys. A371, 1 (1981); Phys. Lett. 106B, 379 (1981).
17. R. B. Firestone, V. S. Shirley, C. M. Baglin, S. Y. Frank Chu and J. Zipkin, *Table of Isotopes*, (Wiley Interscience Publication, 1996).
18. B. S. Pudliner, A. Smerzi, J. Carlson, V. R. Pandharipande, S. C. Pieper and D. G. Ravenhall, Phys. Rev. Lett. 76, 2416 (1996).
19. Z. Ren, M. Mittig, B. Chen, Z. Mu, G. Auger and G. Xu, Phys. Rev. C 52, R1764 (1995).
20. P.-G. Reinhard and H. Flocard, Nucl. Phys. A584, 567 (1995).
21. E. W. Otten, *Treatise on Heavy-Ion Science*, Vol 8, Edited by D. A. Bromley (Plenum Publishing Corporation, 1989) p. 517.
22. B. A. Brown and B. H. Wildenthal, Ann. Rev. Nucl. Part. Sci. 38, 29 (1988).
23. B. A. Brown, C. R. Bronk and P. E. Hodgson, J. Phys. G 10, 1683 (1984).
24. J. Stevenson et al., Phys. Rev. C 37, 2220 (1985).
25. M. Fauerbach et al., Phys. Rev. C 53, 647 (1996).
26. S. Cwiok, J. Dobaczewski, P-H. Heenen, P. Magierski and W. Nazarewicz, Nucl. Phys. A611, 211 (1996).
27. N. V. Zamfir, G. Hering, R. F. Casten and P. Paul, Phys. Lett. B357, 515 (1995).
28. M. Brack, C. Guet and H.-B. Hakansson, Physics Reports, 123, 275 (1985).
29. Y. Alhassid, G. F. Bertsch, D. J. Dean and S. E. Koonin, Phys. Rev. Lett. 77, 1444 (1996).
30. M. Honma, T. Mizusaki and T. Otsuka, Phys. Rev. Lett. 77, 3315 (1996).
31. T. R. Werner, J. A. Sheikh, M. Misu, W. Nazarewicz, J. Rikovska, K. Heeger, A. S. Umar and M. R. Strayer, Nucl. Phys. A597, 327 (1996).
32. A. Arima and F. Iachello, Adv. Nucl. Phys. 13, 139 (1984).
33. D. S. Brenner, N. V. Zamfir and R. F. Casten, Phys. Rev. C 50, 490 (1994).

ON THE RESTORATION OF ISOSPIN PURITY AT HIGH EXCITATION ENERGY

Valentin Sokolov[a] and Vladimir Zelevinsky

One of the questions of primary interest in nuclear physics, especially for experiments with radioactive nuclear beams, is that of existence and purity of simple modes embedded into continuum. Due to the coupling to compound states, simple modes, such as isobaric analog states (IAS) or giant resonances, acquire a damping width ("internal" dynamics). Experimentally, such states reveal enhanced cross sections in specific channels at corresponding resonance energies ("external" dynamics which include direct decay of a simple mode and decays of intrinsic compound states through their own channels). As a rule, such a state is relatively pure in the entrance channel. The isospin purity is violated by the internal mixing [1] when, due to the high background level density, the statistical enhancement of perturbations becomes important. The restoration of isospin purity at high excitation energy was predicted long ago [2,3] and recently confirmed experimentally [4]. The standard formalism [5] of the strength function proceeds as if the states under consideration were stable. We consider the interplay between internal and external dynamics using an effective nonhermitian hamiltonian [6,7] and looking at the system both from "inside" (strength functions and spreading widths) and from "outside" (S-matrix, cross sections and delay times).

A simple basis state $|0\rangle$ has complex energy $\tilde{\epsilon}_0 = \epsilon_0 - (i/2)\gamma_0$ where γ_0 is the direct decay width. Due to the intrinsic coupling V_n to a dense spectrum of compound states $|n\rangle$, the simple state also acquires access to many evaporation channels. For the IAS with isospin $T_>$, we have to consider the background states which belong mainly to $T = T_> - 1$. The isospin mixing occurs through intrinsic interaction [1] so that the decay channels for the decoupled simple mode and evaporation channels for compound states carry different isospins. The complex energies of compound resonances are $\tilde{\epsilon}_\nu = h_\nu - (i/2)\gamma_{ev}, \nu = 1, 2, ..., N$, supposing that the fluctuations of widths are weak so that one can use a typical evaporation width γ_{ev}.

At the decay channels closed, each eigenfunction $|\alpha\rangle$ with energy ϵ_α carries a fraction

$$f^\alpha = |C_0^\alpha|^2 = \frac{1}{1+L^\alpha} = \left[1 + \sum_n V_n^2/(\epsilon_\alpha - h_n)^2\right]^{-1} \tag{1}$$

of the collective strength determined by the weight of the corresponding component C_0^α in the expansion over the basis states,

$$|\alpha\rangle = C_0^\alpha|0\rangle + \sum_{n=1}^{N} C_n^\alpha|n\rangle. \tag{2}$$

The smooth strength function of the simple excitation is defined in terms of the mean level spacing D of background states, $P_0(\epsilon) = [f^\alpha/D(\epsilon)]_{\epsilon_\alpha=\epsilon}$. Assuming [5] a roughly equidistant dense spectrum of h_n and interaction intensities V_n^2 uncorrelated with energies h_n and slightly fluctuating around their mean value $\langle V^2\rangle > D^2$, the strength function has the Breit-Wigner shape with the spreading width given by the golden rule, $\Gamma^\downarrow \equiv \Gamma_s = 2\pi\frac{\langle V^2\rangle}{D}$. This is expected to be a good approximation for the IAS with $\Gamma^\downarrow \leq 100$ keV.

We generalize this procedure for a decaying system. In our schematic although quite generic model, it could be done exactly. The diagonalization of the total non-hermitian hamiltonian leads to $N+1$

complex eigenvalues $\mathcal{E}_j = E_j - (i/2)\Gamma_j$ where the quasistationary eigenstates $|j\rangle$ can be represented as superpositions of decoupled unstable states $|0\rangle, \ldots, |\nu\rangle$,

$$|j\rangle = \tilde{C}_0^j|0\rangle + \sum_\nu \tilde{C}_\nu^j|\nu\rangle. \tag{3}$$

With L_j being the complex analog of the sum in (1), the fraction $\tilde{f}^j = |\tilde{C}_0^j|^2$ of the strength of the simple state $|0\rangle$ carried by the quasistationary state $|j\rangle$ is

$$\tilde{f}^j = \frac{1}{1+L^j} = \frac{\Gamma_j - \gamma_{ev}}{\gamma_0 - \gamma_{ev}}. \tag{4}$$

In other words, the resulting width of the quasistationary state $|j\rangle$ can be found from simple probabilistic arguments,

$$\Gamma_j = \gamma_0 \tilde{f}^j + \gamma_{ev}(1 - \tilde{f}^j), \tag{5}$$

which emerge here as a result of a quantum-mechanical calculation, with no ensemble averaging or transition to a kinetic description. The energy dependence of the strengths is hidden in the secular equation for complex energies. For small $\tilde{f}_j$,

$$\tilde{f}^j = \frac{D}{2\pi|\gamma_0 - \gamma_{ev}|} \ln \frac{(E_j - \epsilon_0)^2 + \frac{1}{4}(\Gamma_s + |\gamma_0 - \gamma_{ev}|)^2}{(E_j - \epsilon_0)^2 + \frac{1}{4}(\Gamma_s - |\gamma_0 - \gamma_{ev}|)^2}. \tag{6}$$

Up to now we concentrated on the "inside" view of a simple unstable mode mixed with complicated fine structure states. The "outside" world was present as a reservoir for irreversible decay through numerous open channels. Now we take a glimpse of the same system from the viewpoint of reaction amplitudes and cross sections where only asymptotic states are observed. The same effective non-hermitian hamiltonian allows one to find the scattering matrix, the scattering wave function, the time delay matrix and to define the normalized probability $p_n^c(E)$ to find the system in the intrinsic state $|n\rangle$ in the "elastic" reaction $c \to c$. The probability $p_0^c(E)$ characterizes the weight of the simple state $|0\rangle$ in the channel c. In the problem of the IAS this quantity measures the isospin purity in a given channel.

The simplest situation corresponds to the stable background states with no direct access to open channels, $\gamma_{ev} \to 0$, when the intrinsic evolution for the reaction in the channel c starts and ends at the simple state. The background states appear only at the intermediate stages of the reaction. Then

$$p_0^c(E) \equiv f(E) = \left[1 + \sum_n \frac{V_n^2}{(E - h_n)^2}\right]^{-1}. \tag{7}$$

This is nothing but the continuous generalization of the strengths $f^\alpha = |C_0^\alpha|^2$ defined by eq.(1) in discrete points ϵ_α of the intrinsic spectrum, $f^\alpha = f(E = \epsilon_\alpha)$. The distribution (7) wildly fluctuates on the fine structure energy scale. With the energy resolution $\Delta E \gg D$, one sees only a smooth behavior coinciding with that of the strength function $P_0(E)$. A probability of the original isospin can be estimated by averaging

over fine structure and taking $\Gamma^{\downarrow} \gg D$,

$$\overline{p_0(E)} = \frac{1}{\pi}\frac{D}{\Gamma^{\downarrow}}, \tag{8}$$

as an inverse number of fine structure states within the spreading width.

The situation changes in the realistic case with many open evaporation channels. If the simple mode and the compound states have no common decay channels, we find instead of (7)

$$p_0(E) \equiv \tilde{f}(E) = \frac{1}{1+L(E)} = \Big[1 + \sum_{\nu} \frac{V_\nu^2}{|E-\tilde{\epsilon}_\nu|^2}\Big]^{-1}. \tag{9}$$

where the function $\tilde{f}(E)$ extends the strength function (4) of the quasistationary states to a running real energy E, and the loop $L(E)$ is the analog of L^j taken at energy E rather than at complex energy $\mathcal{E}_j$. The calculation of the loop function (9) gives

$$L(E) = \frac{\Gamma_s}{\gamma_{ev}} y \frac{(1+x^2)}{1+x^2y^2}, \quad x = \cot\Big(\pi\frac{E}{D}\Big), \quad y = \tanh\Big(\frac{\pi}{2}\frac{\gamma_{ev}}{D}\Big). \tag{10}$$

For a small evaporation width, $\gamma_{ev} \ll D$,

$$L(E) = \frac{\pi\Gamma_s}{2D}(1+x^2). \tag{11}$$

The results in this limit do not depend on the evaporation width and therefore coincide with those following from (7); the weight of the simple state in the intrinsic part of the scattering wave function is of order of $D/\Gamma_s \ll 1$.

As level density and number of open channels increase, the ratio γ_{ev}/D rapidly grows together with the argument of y, eq.(10). One has a fast transition to overlapping background states when $y \approx 1$ and $L(E) \to \Gamma_s/\gamma_{ev}$. The probability (9) in this case is noticeably greater than in (8),

$$\tilde{f} = \frac{\gamma_{ev}}{\gamma_{ev}+\Gamma_s} \gg \frac{D}{\Gamma_s}. \tag{12}$$

The fluctuations disappear, and the simple state preserves its individuality in the intrinsic wave function across the whole region of the giant or analog resonance. This behavior is demonstrated in 1. The purity of the intrinsic part becomes perfect when $\gamma_{ev} \gg \Gamma_s$; the depletion of admixed states of the opposite isospin occurs faster than their population. This gives a microscopic justification of the isospin purity at high excitation energy. At the same conditions, the fraction of the simple mode carried by a generic compound state, $1-\tilde{f} = \Gamma_s/(\gamma_{ev}+\Gamma_s)$, is small; the compound processes have no time to explore the presence of the exceptional simple state.

In conclusion, the analysis confirms the old idea [2,3] of increasing isospin purity at high excitation energy. The experimental data [4] agree with this conclusion. The purity of a simple mode is restored because of the fast depopulation of the admixed background states when their decay width γ_{ev} increases

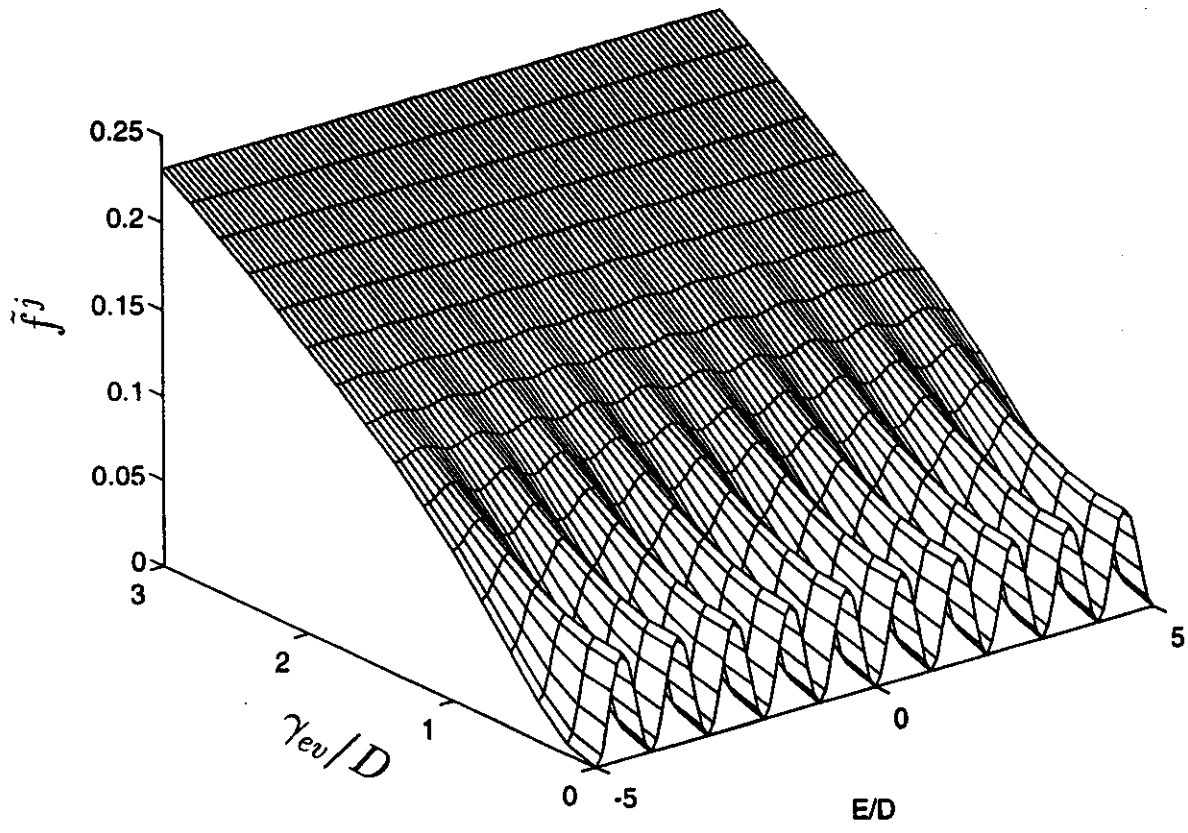

Figure 1: The relative probability $\tilde{f}(E)$ of excitation of a simple state through the channel c as a function of energy, E/D, and the evaporation width, γ_{ev}/D. The value of the spreading width, $\Gamma_s/D = 10$, is chosen for illustrative purposes to make the oscillations along the energy axis clearly seen; the oscillations rapidly disappear as γ_{ev} grows.

compared to the spreading width Γ_s of the simple state (IAS in this case).

a. Permanent address: Budker Institute of Nuclear Physics, Novosibirsk 630090, Russia.

References

1. H.L.Harney, A.Richter and H.A.Weidenmüller. Rev. Mod. Phys. 58 (1986) 607.
2. H.Morinaga. Phys. Rev. 97 (1955) 444.
3. D.H.Wilkinson. Phil. Mag. 1 (1956) 379.
4. K.A.Snover. Nucl. Phys. A553 (1993) 153c.
5. A.Bohr and B.Mottelson, *Nuclear Structure*, vol. I, Benjamin, New York, 1969.
6. C.Mahaux and H.A.Weidenmüller. *Shell-Model Approach to Nuclear Reactions*, North-Holland, Amsterdam, 1969.
7. V.V.Sokolov and V.G.Zelevinsky. Nucl. Phys. A504 (1989) 562.

"DISAPPEARANCE" OF COLLECTIVE STRENGTH AT HIGH EXCITATION ENERGY

Valentin Sokolov[a] and Vladimir Zelevinsky

Open mesoscopic quantum systems are characterized by the presence of "simple" (single-particle and collective) excitations, "complicated" (chaotic) intrinsic motion involving many degrees of freedom, and irreversible decay into continuum. The approach used for studying the isospin purity, see the preceding report [1], considers the internal and external dynamics on equal footing. Here we apply it to the physics of giant resonances (GR) in highly excited nuclei. The new phenomenon of "disappearance" of the collective GDR strength at high excitation energy [2] is still a debatable subject. Its explanation was suggested in [3] in terms of the kinetic balance between the decay and mixing. The authors showed that the probability of excitation of a collective mode in an initially heated nucleus is equal to $\Gamma_s/(\gamma_{ev}+\Gamma_s)$ where Γ_s is the spreading width of the GR and γ_{ev} is the evaporation width of a generic admixed compound state. This probability falls when the temperature exceeds a critical value determined by the condition $\gamma_{ev}\sim\Gamma_s$. We derive the analogous conclusion from a full quantum-mechanical consideration which properly accounts for the fact that the manifestations of the simple mode in the reaction channels are intertangled with the chaotic mixing inside the system.

Using the general results of [1], we compare the cross sections of various processes. They are determined by the reaction matrix $T^{ab}(E)$,

$$\hat{T}(E)=\mathbf{A}^T\mathcal{G}(E)\mathbf{A} \tag{1}$$

where $\mathbf{A}=\{A_n^a\}$ is the set of decay amplitudes from an intrinsic state n (the state $|0\rangle$ is that of the GR) to a reaction channel a while $\mathcal{G}(E)=(E-\mathcal{H})^{-1}$ is the total propagator which includes the continuum coupling through the same amplitudes $\mathbf{A}$. Let the channel c be related to the signal of the GR as a strong collective gamma radiation. If we start with the excitation of the simple mode $|0\rangle$ through A_0^c, the "elastic" scattering, $c\to c$, competes with the evaporation $c\to e$ through numerous compound channels e. The results of the full quantum solution can be summarized as follows.

With no evaporation, the elastic cross section reveals fine structure fluctuations on the scale of the compound level spacing D. In the case of small γ_{ev}/D, these fluctuations are enhanced in a vicinity of the GR centroid $E=\epsilon_0$. The fluctuations are washed away when evaporation becomes strong, $\gamma_{ev}\gg D$, when

$$|T^{cc}|^2=\gamma_0^2\left[E-\epsilon_0+\frac{i}{2}(\gamma_0+\Gamma_s)\right]^{-1}. \tag{2}$$

Here the decay width $\gamma_0=(A_0^c)^2$ and the spreading width Γ_s are combined into the total width of the resonance on the real energy axis. In Fig. 1 we illustrate the energy dependence of the elastic cross section $\sigma^{cc}=|T^{cc}|^2$.

The fraction of $|T^{cc}|^2$ in the total cross section determines the branching ratio of the simple decay mode, see notations in [1],

$$\mathcal{B}^{cc}(E)=\frac{\gamma_0}{\gamma_0+\gamma_{ev}L(E)}=\frac{\gamma_0\tilde{f}(E)}{\gamma_0\tilde{f}(E)+\gamma_{ev}\left[1-\tilde{f}(E)\right]}, \tag{3}$$

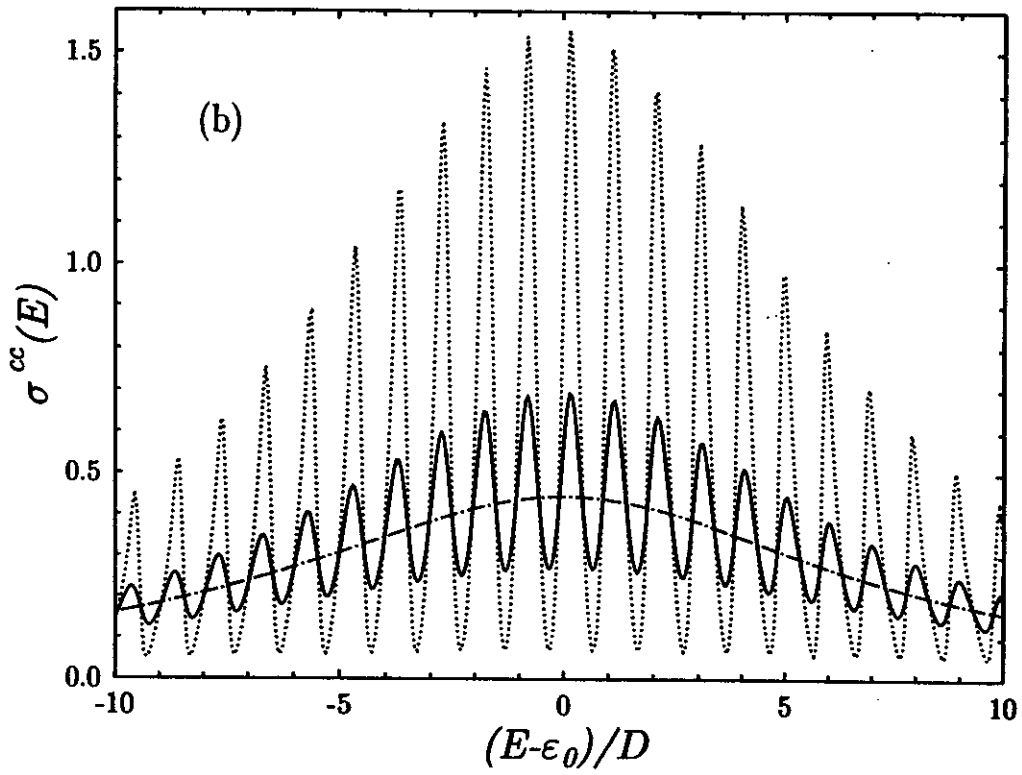

Figure 1: Elastic cross section σ^{cc} in the channel c as a function of energy for $\Gamma_s > \gamma_0$. For illustrative purposes the parameters are $\gamma_0/D = 5$, $\Gamma_s/D = 10$, and $y \equiv \tanh(\pi\gamma_{ev}/2D) = 0.3$ (dots), $y = 0.7$ (solid curve) and $y = 1$ (dash-dotted curve).

in agreement with the probabilistic interpretation of the function $\tilde{f}(E)$. The amplitude $T^{ec}(E)$ for evaporation in a compound channel e after the simple state was excited in the entrance channel c, strongly fluctuates together with the exit amplitudes A_n^e. Assuming $k \gg 1$ uncorrelated statistically equivalent decay channels, we can make an ensemble averaging to obtain the corresponding branching ratio

$$B^{ec} = \frac{1}{k}\frac{\gamma_{ev}L(E)}{\gamma_0 + \gamma_{ev}L(E)} = \frac{1}{k}\frac{\gamma_{ev}\left[1-\tilde{f}(E)\right]}{\gamma_0\tilde{f}(E) + \gamma_{ev}\left[1-\tilde{f}(E)\right]}. \tag{4}$$

In accordance with the unitarity condition, $B^{cc} + kB^{ec} = 1$.

In agreement with [3], at considerable evaporation and overlapping compound resonances, $\gamma_{ev}/D \gg 1$, the branching ratios saturate at

$$B^{cc} = \frac{\gamma_0}{\gamma_0 + \Gamma_s}, \qquad B^{ec} = \frac{1}{k}\frac{\Gamma_s}{\gamma_0 + \Gamma_s}. \tag{5}$$

For the saturated Γ_s, these limiting values are insensitive to the level density of compound states and depend on excitation energy only through the direct width γ_0. Then only the simple state with the total width $\gamma_0 + \Gamma_s$ is seen in the entrance channel c. The background of compound states serves as a reservoir for irreversible decay, equivalent by its properties to decay into continuum.

The processes started in the compound channels e, for example, driven by a nuclear interaction of heavy ions, can populate the GR through internal mixing. The corresponding amplitude T^{ce} is the same as T^{ec} considered above. The competing compound-compound processes include the virtual excitation of the GR with the subsequent deexcitation again via compound channels. The statistical averaging gives the branching ratio for the deexcitation into the channel c carrying the signature of the GR,

$$B^{ce} = \frac{1}{2\pi} \frac{\gamma_0 \Gamma_s}{(E-\epsilon_0)^2 + (\gamma_0 + \Gamma_s)/4} \frac{D}{\gamma_{ev}}. \tag{6}$$

The GR is suppressed by the inverse number γ_{ev}/D of the background states on the typical evaporation width. The observation of the signal of the GR in the reaction started in a compound channel becomes less probable with increasing γ_{ev}, in agreement with the kinetic arguments of [3].

One of the objections raised against the kinetic explanation is related to the possibility of preequilibrium, for example electromagnetic, excitation of the GR [4] when the intrinsic evolution starts with the state which already carries some amount of collective strength. This means the presence of the reaction channels a connected both to the simple mode and to the background states. For such channels, all amplitudes, A_0^a and A_n^a, do not vanish; until now we assumed that, before the internal mixing, the GR and the fine structure states have no common decay channels. For the case of the IAS, this situation is associated with the external isospin mixing which is apparently of minor importance [5]. However, for the GR this effect should be incorporated into theory.

The corresponding amplitudes will be denoted as a_0 and a_n for the GR and background states, respectively. The reaction starts in the channel a and ends either in the channel c specific for the GR or in any of the other channels, a or e. Similar to the amplitudes A_n^e, the new amplitudes a_n are uncorrelated quantities with a magnitude $\langle a^2 \rangle \equiv \gamma_a \sim \gamma_{ev} \gg D$. The calculation of the elastic amplitude T^{aa} and the deexcitation amplitude T^{ca} through the special channel c determines

$$\frac{\langle |T^{ca}|^2 \rangle}{\langle |T^{aa}|^2 \rangle} \approx \left(\frac{D}{\pi \gamma_a} \right)^2 \gamma_0 \gamma_0^a |\mathcal{G}_{00}|^2 \tag{7}$$

where the squared propagator $|\mathcal{G}_{00}|^2$ determines the energy shape of the Breit-Wigner type. The average partial width for the decay of the simple state into the channel a is equal to $\gamma_0^a \equiv \langle |\alpha_0|^2 \rangle = a_0^2 + (\gamma_a/\gamma_{ev})\Gamma_s$. Thus, in the case of the common channel populating both, simple and compound, states, the statistical branching for the deexcitation via the GR drops with the increasing level density $\rho \sim 1/D$ of compound states. Whence, strong common channels with $\gamma_a \sim \gamma_{ev}$ cannot recover the disappearing simple mode. Weak channels, $\gamma_a \simeq \gamma_{ev}/k$, are useless because of their small total cross sections.

In conclusion, the general quantum-mechanical analysis confirms the qualitative explanation [3] of the disappearance of the collective GDR strength as a result of a shift of the kinetic equilibrium in favor of compound decays when the ratio γ_{ev}/Γ_s increases. Moreover, the conclusion is still valid when the GR can be excited from the reaction channels which are common for the GR and the background states. To complete the analysis, one needs to consider the situation when several simple states share the collective strength and the decay width into the signal channel c. In the realistic GDR calculation, this "configuration splitting" leads to specific interference phenomena [6]. The distribution of the dipole strength and the width evolves with excitation energy; typically, this results in the quenching of the collective strength and

its redistribution in favor of the low energy component. These effects are seen experimentally [7] and discussed in detail in [8].

a. Permanent address: Budker Institute of Nuclear Physics, Novosibirsk 630090, Russia.

References

1. V.Sokolov and V.Zelevinsky, this Annual Report.
2. J.J.Gaardhøje. Ann. Rev. Nucl. Part. Sci. 42 (1992) 483.
3. P.F.Bortignon, A.Bracco, D.Brink, and R.A.Broglia. Phys. Rev. Lett. 67 (1991) 3360.
4. Ph.Chomaz. Nucl. Phys. A569 (1994) 203c.
5. H.L.Harney, A.Richter and H.A.Weidenmüller. Rev. Mod. Phys. 58 (1986) 607.
6. V.V.Sokolov and V.G.Zelevinsky. Fizika 22 (1990) 303.
7. Ph.Chomaz and N.Frascaria. Phys. Rep. 252 (1995) 275.
8. V.V.Sokolov, I.Rotter, D.V.Savin and M.Müller. Preprints FZR-153,154. Rossendorf, 1996.

GAMOW-TELLER STRENGTH AS A FUNCTION OF EXCITATION ENERGY

Njema Frazier, B. Alex Brown, D. J. Millener [a] and Vladimir Zelevinsky

We have studied Gamow-Teller (GT) transitions between highly excited states in the *sd*-shell. Since the pioneering work by Wigner 60 years ago [1], spin-isospin symmetry and the properties of nuclear interaction related to the GT strength have been studied in detail [2]. From the considerable work carried out for low lying states (see for example [3]), it is apparent that full $0\hbar\omega$ shell-model calculations (presently possible up to $A \sim 50$[4]) provide an excellent description of measured GT matrix elements apart from an overall quenching of the free GT operator ($g_A = 1.26$) corresponding to $g_A^{eff} \sim 1$. This quenching is attributed both to excitation to configurations outside of the $0\hbar\omega$ shell-model space and to delta-isobar excitations [5]. However, the study of GT transitions from excited states remains virtually non-existent. Such calculations can give us important information about the behavior of a simple excitation mode in a realistic environment of incoherent nuclear interactions (the evolution of the isospin-invariant pairing as a function of excitation energy was discussed in [6]).

The GT operator is defined as a sum over the nucleons of the $\sigma\tau$ operator:

$$O_\mu^{(\pm)} = \sum_{nucleons} \sigma_\mu t_\pm = \sum_{k,k'} (\sigma_\mu t_\pm)_{k,k'} a_k^\dagger a_{k'} \tag{1}$$

where the last term is given in second quantized form, k represents a complete set of single-particle quantum numbers including the isospin projection, and $\pm$ corresponds to the $\beta^\mp$ direction for the transition. The operator $t_\pm$ converts a neutron into a proton and vice versa ($t_\pm = \mp 1/\sqrt{2}\tau_\pm$ where $\tau_\pm$ are the spherical components of $\tau = 2t$). The GT strength is obtained by calculating the matrix element squared for the $\langle f|O^\pm|i\rangle$ transition between the many-body eigenstates $|i\rangle$ and $|f\rangle$. We study the strength function summed over all final states $|f\rangle$ to give the *total* GT strength, B_{GT}, of the initial state $|i\rangle$,

$$B_{GT}^{(\pm)}(i) = \sum_f B_{GT}^{(\pm)}(i \to f) = \sum_f \sum_\mu |\langle f|O_\mu^{(\pm)}|i\rangle|^2 = \sum_\mu \langle i|O_\mu^{(\pm)\dagger} O_\mu^{(\pm)}|i\rangle \tag{2}$$

where the closure summation over $|f\rangle$ was used. According to the GT sum rule which follows from the definition (2), the difference in total strength $B_{GT}^{(+)}(i) - B_{GT}^{(-)}(i) = 3(N_i - Z_i)$ is directly related to the number of protons and neutrons in the initial nucleus. For the $T = 0$ states of an $N = Z$ nucleus, which we use as an example in our study, it suffices to consider one of these sums, say $B_{GT}^{(-)} \equiv B_{GT}$.

We compute the GT strengths for a system of $n = 8$ valence nucleons in the *sd*-shell which can be seen as a subset of states in the ^{24}Mg nucleus. Using a realistic hamiltonian, we find the eigenfunctions $|J^\pi T\rangle$ with the exact quantum numbers of angular momentum and isospin and use them to calculate the amplitudes for the GT transitions. The Wildenthal hamiltonian [5, 7] defines the single-particle energies and the interaction between the valence particles by fitting more than 400 binding and excitation energies for the *sd*-shell nuclei. The total GT strength (2) is shown in Fig. 1(a) as a function of excitation energy for all 325 individual $J^\pi T = 0^+0$ states in ^{24}Mg found in the *sd* shell model. We see a clear monotonic increase in the total B_{GT} strengths with excitation energy.

We now look for an understanding of the above result, obtained by explicit summation over shell-model final states, in terms of either statistical ideas or in the limit of well-defined symmetries for

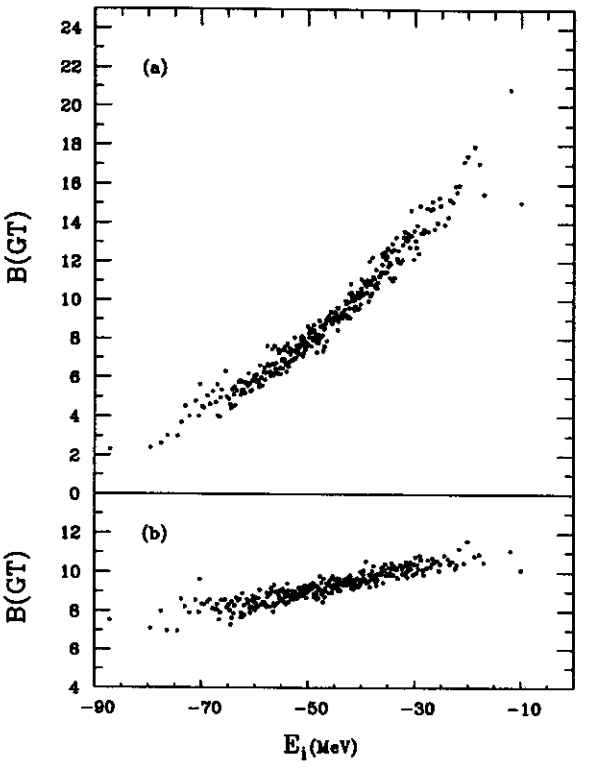

Figure 1: (a) The total Gamow-Teller strength from the 0^+ states of ^{24}Mg plotted as a function of the absolute energy of the 0^+ state. (b) The total strength obtained from the incoherent sum over the partial contributions from each term pair of single-particle states.

the shell-model states. The structure of the shell-model eigenstates is determined largely by competition between the central and spin-orbit components of the effective interaction. The spin-orbit interaction enters mainly at the one-body level by splitting the energy of the single-particle states with the same orbital momentum ($d_{5/2}$ and $d_{3/2}$ in our case). The central interaction is largely $SU(4)$ conserving, as can be demonstrated by turning off the other components of the interaction, and the appropriate basis is the Wigner supermultiplet scheme characterized by a Young tableaux $[f]$, quantum numbers $(\lambda\mu)$ of the $SU(3)$ group, orbital L, spin S and total angular momentum J, isospin T and additional quantum numbers for multiple occurrences of L or TS. The [2222] symmetry ([44] spatial symmetry) ground state has $B_{GT} = 0$. On the other hand, the spin-orbit interaction alone leads to pure jj coupling and a $d^8_{5/2}$ ground state with seniority zero has $B_{GT} = 112/15$ (6/7 of this from $d_{5/2} \rightarrow d_{3/2}$ transitions).

First we consider a statistical treatment within the framework of the jj coupling scheme. The matrix element $\langle f|O|i\rangle$ of any one-body operator between complicated many-body states is the coherent sum of the products of single-particle matrix elements, $(l, j||\sigma_\mu t_-||l, j')$ in our case, and the one-body transition densities $\langle f||a^\dagger_{lj}a_{lj'}||i\rangle$. (the GT operator does not change the orbital momentum l). The non-zero values for the sd-case correspond to the following (lj, lj') transitions: $(d_{5/2}, d_{5/2})$, $(d_{5/2}, d_{3/2})$, $(d_{3/2}, d_{3/2})$, $(d_{3/2}, d_{5/2})$, and $(s_{1/2}, s_{1/2})$. Assuming that the very complicated eigenstates have nearly random phases for its components [6, 8], we can substitute the one-body transition densities by their mean values for the heated Fermi-liquid, $\sqrt{n_{lj'}(1-p_{lj})}$, in terms of the mean neutron, n, and proton, p, occupation probabilities to

experiment [7]. The calculation by Poppelier *et al.* [2] had the excited $\frac{3}{2}^-$ state at 21.96 MeV. Their result also showed an excited $\frac{5}{2}^+$ state at 2.68 MeV, a $\frac{1}{2}^-$ state at 4.58 MeV, and a $\frac{3}{2}^+$ state at 3.13 MeV. It is important to note that all excited states in ^{11}Li are broad continuum states, and their energies in our shell model are accurate to within 1 MeV.

The ground state wave function of ^{11}Li in our model is $62.71\%\,|0\hbar\omega) + 37.29\%\,|2\hbar\omega)$. This wave function contains a substantial admixture of $2\hbar\omega$ components, of which 19.62% come from the pure $(0d)^2$ configurations and of which 10.02% arise from the pure $(1s)^2$ configurations.

Our methods of analyses of the elastic and inelastic proton scattering data follows those we used in analyses of the elastic and inelastic scattering data from 200 MeV protons on ^{12}C [9] and on ^{6,7}Li [10]. Those analyses are based upon an effective nucleon–nucleon (NN) interaction in coordinate space that has been obtained from an accurate mapping of the (NN) g matrices of the Paris NN interaction [11] for infinite nuclear matter obtained from solving the Bruckner-Bethe-Goldstone equations [12]. That complex interaction is both energy and density dependent. Folding the effective interaction with the target density matrix elements then yields energy dependent, complex and nonlocal nucleon–nucleus (NA) optical potentials in which is contained the density dependence required to describe well, without renormalisations, both elastic and inelastic scattering data [9]. The latter have been calculated in the distorted wave approximation (DWA) in which the same effective interaction is the transition operator and the distorted waves are obtained from the microscopic optical potentials. The interaction at 65 MeV also has been used in analyses of proton elastic and inelastic scattering from diverse targets [13], wherein very good agreement with cross section and polarization data has been obtained. The code DWBA91 of Raynal [14] has been used to calculate all of the elastic and inelastic scattering cross sections.

Specification of the single particle wave functions is important in analyses of scattering data. This is especially true for the scattering from ^{11}Li, as that halo nucleus requires single particle wave functions that reproduce the density extending to large radii. Such is not the case for ^{9}Li. We have used HO and WS single particle wave functions in the calculations. As there are no electron scattering data by which to set the wave functions, the WS parameter values were determined from fits to the longitudinal elastic electron scattering form factors for either ^{7}Li [10] (a choice predicated on the similarity of charge) or ^{9}Be [15] (a choice predicated on mass). However, for the scattering with ^{11}Li the WS functions were adjusted to define the halo nature of that nucleus. Specifically we used WS wave functions with a binding energy of 500 keV for the halo neutron orbits, namely the $0p_{\frac{1}{2}}$ orbit and the $0d1s$ and $0f1p$ shells in the complete $(0+2)\hbar\omega$ shell model space. The problem of choosing appropriate radial wave functions for transitions between loosely bound states has been illuminated (and resolved) by Millener *et al.* [16] for the case of ^{11}Be.

The results of the calculations made for the elastic scattering of 62 and 68 MeV protons from ^{11}Li, and of 62 MeV protons from ^{9}Li are shown in Fig. 1. Therein the data for 62A MeV [5] and 68A MeV [7] ^{11}Li scattering from hydrogen are compared in the top panel of Fig. 1 to the result at 62 MeV made using the WS wave functions (^{9}Be set, solid line), and also to that at 68 MeV (dashed line). The result of calculation of the scattering from ^{11}Li made at 62 MeV using harmonic oscillators is displayed as the dot-dashed line. It overestimates the cross section significantly, and illustrates the need for specifying the halo density distribution appropriately. The results of the calculations using the WS single-particle wave functions are insensitive to changing the binding energy of the halo orbits to as low as 50 keV. The data for the elastic scattering of 62A MeV ^{9}Li from hydrogen [5] and the results of calculations made using the WS wave functions are compared in the bottom panel of Fig. 1, wherein the results obtained using the ^{9}Be

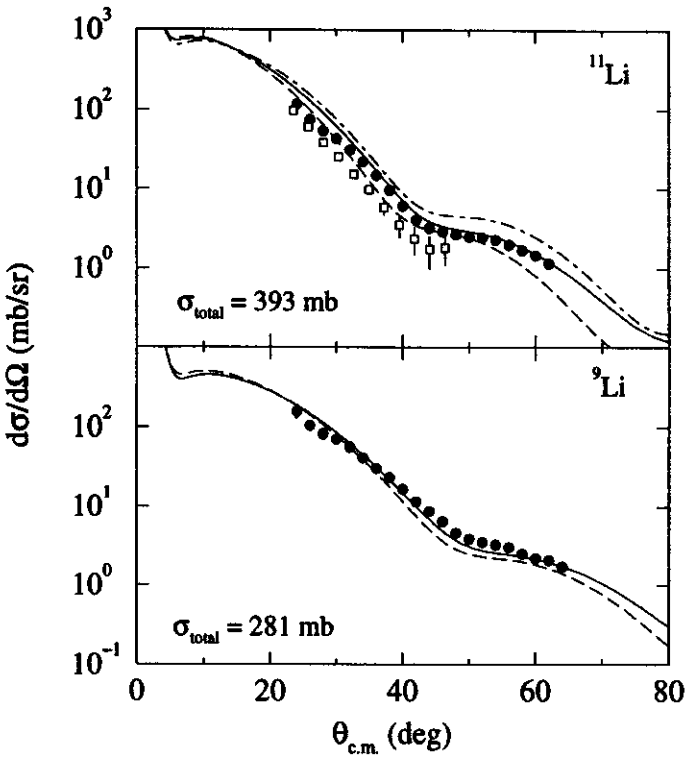

Figure 1: Elastic scattering of 60 and 68 MeV from ^{11}Li (top) and ^{9}Li (bottom). The data of Moon *et al.* [5] (circles) and of Korsheninnikov *et al.* [7] (squares) are compared to the results of the calculations made using the $(0+2)\hbar\omega$ and $(1+3)\hbar\omega$ shell model wave functions. The results for the scattering from ^{11}Li at 60 MeV used both the ^{9}Be WS (solid line) and HO single particle wave functions (dot-dashed line). The result at 68 MeV using the WS wave functions is displayed by the dashed line. The result for the scattering from ^{9}Li using the ^{7}Li set of WS wave functions is displayed by the dashed line.

and ^{7}Li sets are displayed by the solid and dashed lines respectively. There the use of the ^{9}Be set of WS functions is closer in agreement with the data, although the ^{7}Li set provides a reasonable respresentation. In the case of ^{11}Li, the results using both WS sets are quite similar, and hence only the ^{9}Be results are displayed. The excellent agreement with experiment for both nuclei confirms the conclusion by Crespo *et al.* [17] of the need for the specification of the full structure of the ^{9}Li core.

The total nuclear elastic scattering cross sections from ^{9}Li and ^{11}Li are 281 and 393 mb, respectively. This is in seeming disagreement with Moon *et al.* [5], who interpreted their experiment as indicating a significant decrease in cross section from ^{9}Li to ^{11}Li. Our result is due to the contributions made from the cross section values at the (unobserved) forward angles for ^{11}Li and is what should be expected: the larger size of ^{11}Li leads to a narrower and more intense diffraction pattern.

The data for the inelastic scattering of 68 MeV protons from ^{11}Li [7] are compared with the results of our calculations in Fig. 2(a) and neither the shapes nor the magnitudes agree. It is a possibility that the a problem may lie in our choice of wave functions for the excited states. It is also possible that our approach does not guarantee proper treatment of excitations in the continuum. Also, as the excited (continuum) states are broad, the excitation of many higher lying states may contribute to the inelastic cross section.

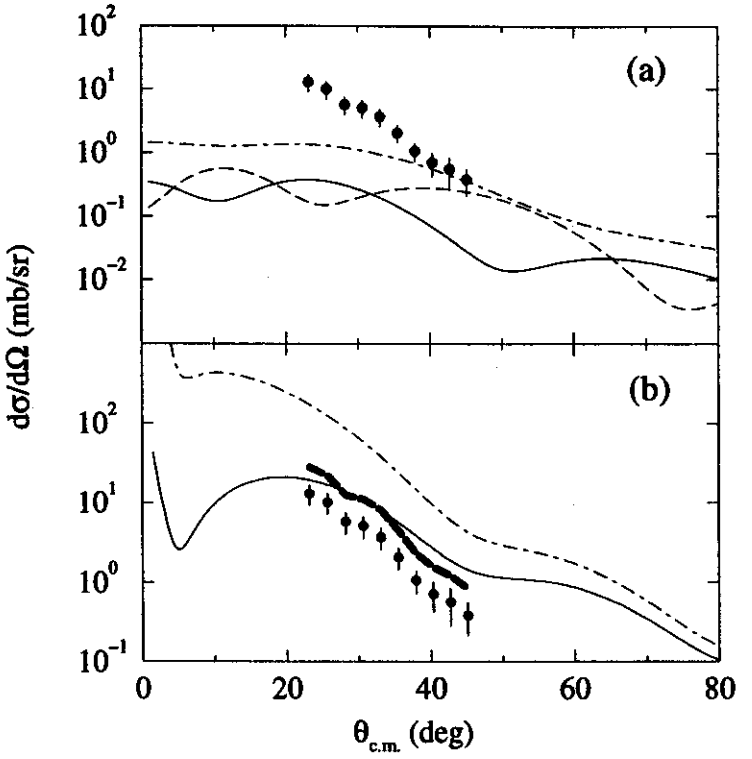

Figure 2: Comparison of the inelastic 68 MeV proton scattering data [7] with (a) the results of the calculations made assuming the transition to the $\frac{3}{2}^-$ (1.49 MeV) (solid line), the $\frac{3}{2}^+$ (1.83 MeV) (dashed line), and the $\frac{1}{2}^-$ (1.87 MeV) (dot-dashed line) states, and (b) the result of the calculation assuming the shake-off mechanism (solid line). The dashed line in (b) is the measured inelastic cross section of [7] rescaled under the assumption that the total observed energy spectrum of that experiment represents shakeoff. The elastic scattering of 68 MeV protons from ^{9}Li is displayed by the dot-dashed line.

Hence we propose a simpler model, incorporating the excitation of the continuum as a whole.

The basic process is elastic scattering of the proton from the ^{9}Li core [18]. The momentum imparted to the halo in the new center-of-mass system entails a certain probability of breakup into the constituents $^9\mathrm{Li}+n+n$. Such processes are commonly encountered in atomic physics, where they are referred to as "shake–off". Another analogy is the recoilless absorption of photons in the Mössbauer effect, where the probability that the struck system remains in its ground state is referred to as the Debye-Waller (DW) factor.

The differential cross section for inelastic scattering was calculated as the product of P_s and the differential cross section for elastic scattering from ^{9}Li. Its total amounts to 20 mb. From Fig. 2(b) it is seen that this calculation agrees well with the inelastic scattering results at 68 MeV [7]. The experimental points with error bars refer to an assumed narrow and symmetric interval around the 1.3 MeV peak. The experimental energy spectrum in [7] shows a pronounced tail towards higher energies, and if the cross sections are rescaled to include this, the agreement is improved. Indeed, an asymmetric shape for the shakeoff is expected from our estimates and also from calculations and measurements of Coulomb shakeoff [19].

In conclusion, there does not seem to be any compelling evidence from the proton scattering experiments of Korsheninnikov *et al.* [6,7] for a 1.3 MeV excited level in ^{11}Li. The asymmetric energy spectrum observed in those experiments seems to be essentially the result of the elastic scattering from the ^{9}Li core leading to shakeoff. Our interpretation of the observed structure as an effect of nuclear–shakeoff is not in conflict with a shell model nor an alternative to it. Dynamic effects of this kind should appear naturally if the transition in the spectrum from bound to continuum states is included explicitly. However, states are predicted in the shell model in the region 1–2 MeV. Such states may be observed in single-nucleon transfer experiments.

a. School of Physics, University of Melbourne, Parkville, Vic. 3052, Australia

References

1. H. G. Bohlen *et al.*, Z. Phys. A 351, 7 (1995).
2. N. A. F. M. Poppelier, L. D. Woods, and P. W. M. Glaudemans, Phys. Lett. 157B, 120 (1985).
3. E. K. Warburton and B. A. Brown, Phys. Rev. C 46, 923 (1992).
4. H. Sagawa, B. A. Brown, and H. Esbensen, Phys. Lett. 309B, 1 (1993).
5. C.–B. Moon *et al.*, Phys. Lett. 297B, 39 (1992).
6. A. A. Korsheninnikov *et al.*, Phys. Rev. C 53, R537 (1996).
7. A. A. Korsheninnikov *et al.*, Phys. Rev. Lett. 78, 2317 (1997).
8. OXBASH-MSU (the Oxford-Buenos-Aries-Michigan State University shell model code), A. Etchegoyen, W. D. M. Rae, and N. S. Godwin (MSU version by B. A. Brown, 1986); B. A. Brown, A. Etchegoyen, and W, D. M Rae, MUSCL Report No. 524, 1986 (unpublished).
9. S. Karataglidis, P. J. Dortmans, K. Amos, and R. deSwiniarski, Phys. Rev.. C 52, 861 (1995).
10. S. Karataglidis, B. A. Brown, K. Amos, and P. J. Dortmans, Phys. Rev. C, in press (1997).
11. M. Lacombe, B. Loiseau, J. M. Richard, R. Vinh Mau, J. Côté, P. Pirés, and R. de Tourreil, Phys. Rev. C 21, 861 (1980).
12. P. J. Dortmans and K. Amos, Phys. Rev. C 49, 1309 (1994).
13. P. J. Dortmans, K. Amos, and S. Karataglidis, University of Melbourne Internal Report, UM–P–97/13, 1997 (unpublished).
14. J. Raynal, computer code DWBA (NEA 1209/02).
15. P. J. Dortmans, K. Amos, and S. Karataglidis, J. Phys. G 23, 183 (1997)
16. D. J. Millener, J. W. Olness, E. K. Warburton, and S. S. Hanna, Phys. Rev. C 28, 497 (1983).
17. R. Crespo, J. A. Tostevin, and I. J. Thompson, Phys. Rev. C 54, 1867 (1996).
18. There must also be a contribution from quasi-elastic scattering on the halo neutrons. This process has an appreciable cross section but contributes only at high (apparent) excitation energies (10-30 MeV).
19. A. Pushkin, B. Jonson, and M. V. Zhukov, J. Phys. G 22, L95 (1996); H. Esbensen and G. F. Bertsch, Nucl. Phys. A542, 310 (1992).

DEFORMATIONS OF THE NEUTRON-RICH Mg ISOTOPES

Hiroshi Noto[a] and B. Alex Brown

Exotic nuclei exhibit many intriguing aspects of nuclear structure. One of the regions of interest is that for the neutron rich nuclei in the sd-shell far from the stability line. The availability of radioactive beams has renewed the interest in the structure problems to be resolved in this region. The shell closure at neutron number equal to 20 seems to be smeared out in the Na and Mg isotopes. Very recently new experimental data[1] have made clear the enhanced B(E2) value in ^{32}Mg which the simplest sd shell-model calculations[2] failed to reproduce. To overcome their inadequacies, the large-scale shell-model calculations[3,4,5] were carried out which include higher excitations from the sd-shell to the pf-shell. Those calculations have pointed out the importance of $2\hbar\omega$ 2p-2h neutron excitations to the pf-shell. The necessity of inclusion of higher major shell components strongly suggests the possibility of larger deformations around ^{32}Mg, the so-called "island of inversion".

The purpose of this report is to investigate the stability of the deformed single-particle field for the most neutron rich Mg isotopes on the basis of the deformated oscillator model. We hope that such calculations will provide some simple insight into the conventional shell-model methods as well as perhaps indicating their limitations and how they might be improved.

We adopt here the deformated oscillator model in the stretched coordinate representation.[6,7] In this scheme the single-particle basis states themselves are the eigenstates of the spacial part of the deformed single-particle hamiltonian. We obtain the single-particle energies in the deformed oscillator potential by diagonalizing the single-particle hamiltonian with use of the stretched coordinate basis. We assume axial symmetry. We take the harmonic-oscillator energy as $\hbar\omega_o/[1-(\epsilon^2/3)-(2\epsilon^3/27)]^{1/3}$ where $\hbar\omega_o = 41A^{-1/3}$ and the denominator is the volume conserving factor. The total energies of the systems are obtained as the sum of the single-particle energies in the deformed potential. We can get the optimum deformation parameters by searching the lowest total energy values in their respective isotopes. The B(E2) values are calculated by using the wave functions with the optimum deformations in each isotope.

A preferred parameter set for the deformed oscillator is obtained by adjusting the strength of the ℓ^2 force and the energy gap between the major oscillator shells under the conditions; (1) that most of the Mg isotopes should have prolate deformations except ^{26}Mg and ^{30}Mg which are expected to have negative intrinsic Q-moments[8]; and (2) that the gap energies between the sd-shell and the pf-shell in the spherical limit should not largely deviate from those in the shell-model calculations[3] (which are obtained from fits to the experimental binding energies). The second condition is rather crucial, because the oscillator model is not appropriate for determining the gap energies between the major shells. In order to be more realistic the higher major shells are shifted down by 16% compared to the original gap energies. The paramters used in Eq. (5-10) of Ref 7 are $v_{ls} = 0.10$ and $v_{ll} = 0.033$.

The total energy obtained as a function of the deformation parameter ϵ and the mass number A is shown in Fig. 1. From the variation of the total energy with deformation for the Mg isotopes we find that the magnitude and sign of the optimum deformations (lowest energy) varies with the neutron number. In ^{32}Mg the energy surface becomes very flat over a wide range of the deformation. Thus a unique deformation parameter could not be obtained in this isotope. It should be stressed that the present results depend upon only two parameters. The strength of the ℓ^2 interaction and the shell gap.

The B(E2) indicate the amount of collectivity developed in the wave functions. The B(E2;$0^+ \rightarrow 2^+$)

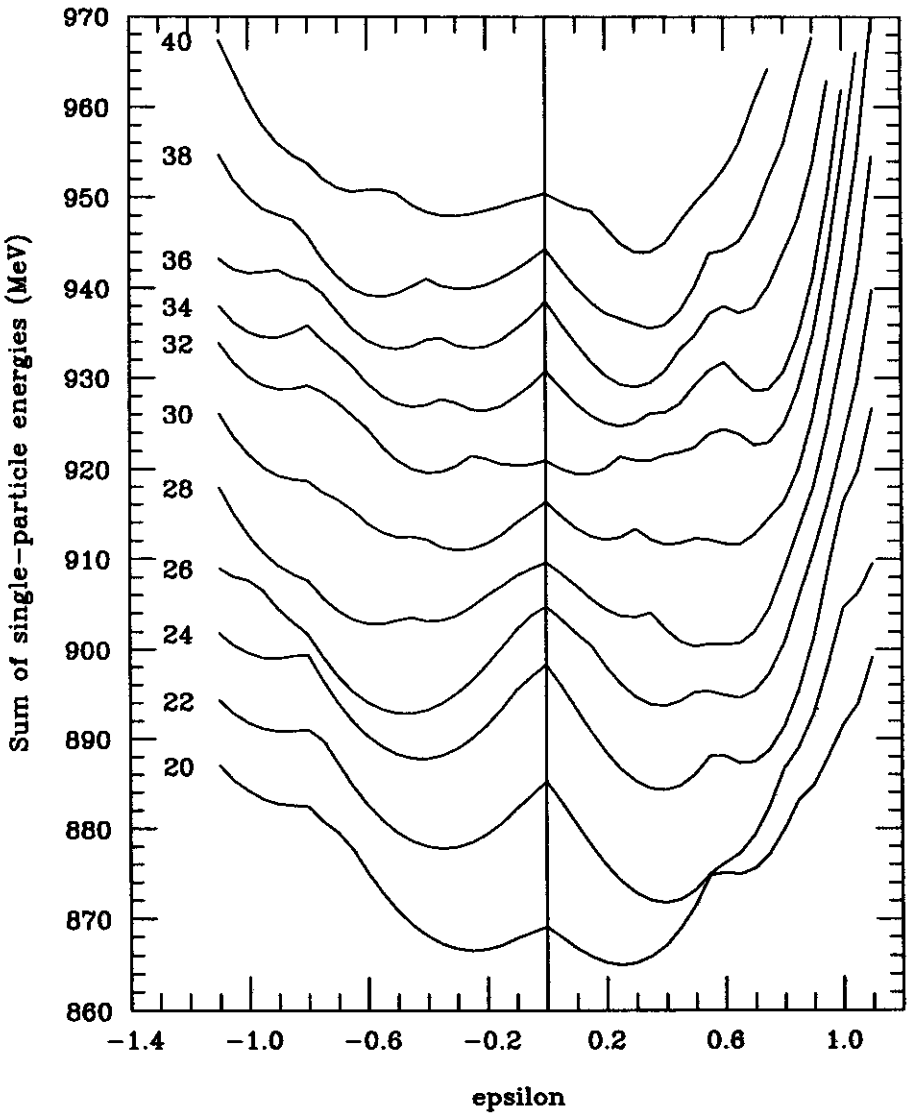

Figure 1: Total energy as a function of the deformation ϵ. The energies are arbitrarily shifted relative to ^{24}Mg.

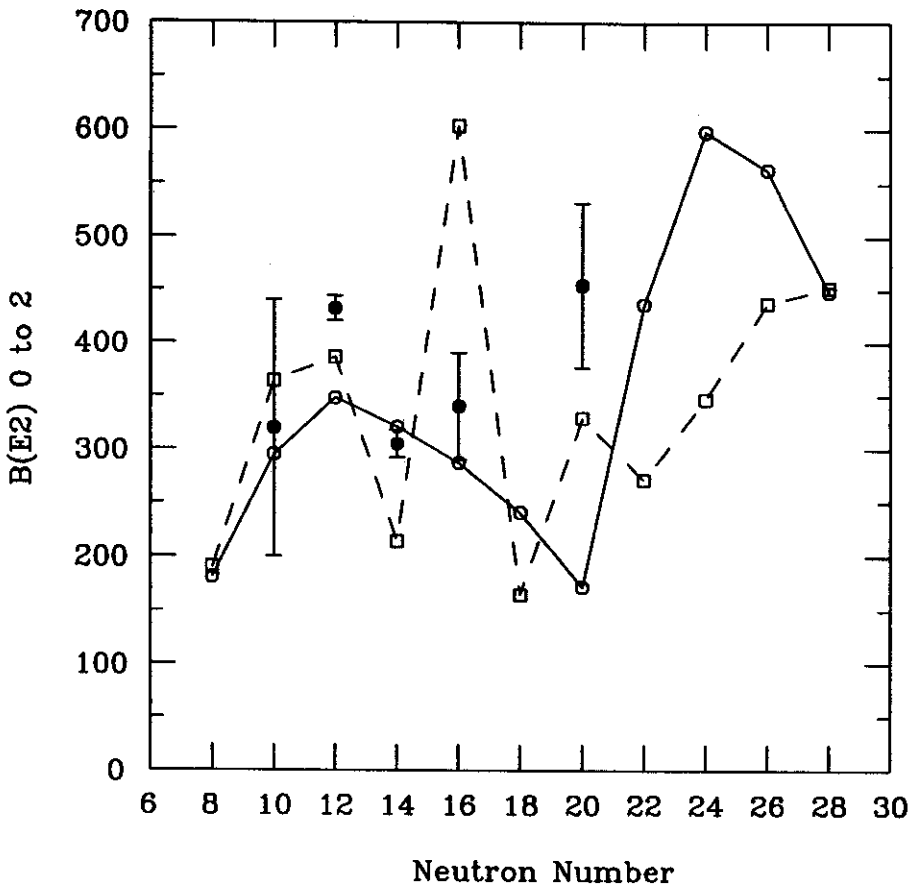

Figure 2: $0^+ \rightarrow 2^+$ B(E2) values (in units of e^2fm^4). The circles connected by a line are the shell-model results. The squares connected by a dashed line are the deformed-oscillator results, and the filled circles with error bars are experiment.

values are calculated with intrinsic states corresponding to the optimum deformations in the adiabatic approximation for each isotopes, except for ^{32}Mg, where the intrinsic state consists of a linear combination of wave functions corresponding to the three local minima (at $\epsilon = -0.4$, $\epsilon = 0.15$ and $\epsilon = 0.7$) with equal weights and with their mutual overlaps neglected.

The results are displayed in Fig. 2, along with the experimental values and the conventional shell-model values based upon the sd-shell wavefunctions[2] for N$\leq$20 and the sd-pf wave functions[3] for N>20. Comparing the present results with the shell-model ones we may point out the following: (1) The basic feature in the shell model is that the isotopes at the magic numbers have a suppressed collectivity: ^{20}Mg, ^{32}Mg (major shell closures) and ^{40}Mg (a semi-major shell closure). The shell-model calculations which take into account $2\hbar\omega$ neutron excitations to the pf-shell for N=20 (the intruder components) give enhanced values closer to experiment[3,4,5] (these calculations are not shown in Fig. 2). (2) In the deformation model ^{32}Mg has a very flat energy surface (see Fig. 1) and the shell disappears. Due to the coexistence of almost spherical, oblate and prolate solutions: a kind of "vibration-like structure" seems to be realized. The enhancement obtained in the deformation model comes from the coexistence of these solutions. In particular there is contribution from a very prolate (ϵ=0.7) solution corresponding to the excitation of four particles from the sd to the fp shell, which is not present in the $2\hbar\omega$ shell-model calculations.

Throughout these Mg isotopes, the lowering of pf-shell and sdg-shell, particularly the former, plays

an important role in the energy gain and in the manifestation of the collectivity. A new shell structure might well be formed around the "island of inversion". Within our model there are several future problems that need to be considered: (1) We need to take into account the Coulomb field and the difference between the average proton-neutron and neutron-neutron interactions by treating the proton shells and the neutron shells explicitly. (2) We need to guarantee the gross saturation properties of the nuclei under consideration by using some macroscopic model. (3) We need to obtain the explicit wavefunctions built on the excited states. (4) We should release the restriction of axial symmetry.

In conclusion we have shown that the gross trends in the deformation properties for the most neutron-rich Mg isotopes follow from the lowest energy configurations of the deformed oscillator model. In the conventional shell model, one is restricted to only one or two spherical oscillator shells, and the effects of the higher shells have to be put in explicitly in terms of effective charges.[9] In this respect the deformed oscillator model is more complete since it incorporates many major spherical oscillator shells, and no effective charge is needed.

a. Hokusei Gakuen University

References

1. T. Motobayashi et al., Phys. Lett. B346(1995)9.
2. B.H. Wildenthal and B.A. Brown, Annu. Rev. Nucl. Sci. 38(1988)29.
3. E.K. Warburton, J.A. Becker and B.A. Brown, Phys Rev. C 41(1990)41.
4. N. Fukunishi, T. Otsuka and T. Sebe, Phys. Lett. B296(1992)279.
5. A. Poves and J. Retamosa, Nucl. Phys. A571(1994)221.
6. S.G. Nilsson, Mat. Fys. Medd. Dan. Vid. Selsk. 29(1955)1.
7. A. Bohr and B. R. Mottelson, Nuclear Structure Vol II, (W. A. Benjamin, Inc, 1975) p. 219 Eq. (5-10).
8. P. Moeller, J. R. Nix, W. D. Myers and W. J. Swiatecki, Atomic Data Nucl. Data Tables 59, 185 (1995).
9. B. A. Brown, A. Arima and J. B. McGrory, Nucl. Phys. A277, 77 (1977).

GAMOW-TELLER STRENGTH IN THE BETA DECAYS OF ^{36}Ca AND ^{37}Ca

B. Alex Brown

During the last few years improvements in experimental techniques have permitted detailed studies of the β-decays of very proton-rich nuclei [3]. Characterized by high energy releases, these decays reveal the GT strength function for transitions covering a large range of excitation energies in the daughter nuclei. They therefore provide opportunities for stringent tests of shell-model calculations. In this report I summarize the the status of the calculations for the recently measured decays of ^{37}Ca [4, 6] and ^{36}Ca [5, 6].

Since our comparison relies upon two different effective hamiltonians for the upper end of the *sd*, we will first we present a short review their development. By the mid 1960's Kuo and Brown had calculated renormalized G-matrix elements for the *sd* shell [7, 8]. One set of matrix elements was applicable to the A = 18 nuclei with two *sd*-shell particles outside of an ^{16}O closed shell [8], and another set was applicable to the A = 38 nuclei with two *sd*-shell holes within a ^{40}Ca closed shell [9]. These G-matrix elements gave qualitative agreement with the experimental A = 18 and A = 38 spectra. When the G-matrix was used to calculate the spectra for the *sd*-shell nuclei with more than two particles or holes, the agreement with the number of observed states was good, but the agreement with the actual energy spectra became worse as the number of particles or holes was increased. The calculated spectra for all these nuclei can be improved by allowing some of the 63 *sd*-shell two-body matrix elements to be parameters in a fit to the experimental energy levels. In general, some linear combinations of these 63 parameters are well determined by the experimental data whereas others are not. By 1977 Chung and Wildenthal [10] had found a "particle" interaction (CWP) for the lower *sd* shell by varying 30 linear combinations of the two-body matrix elements to fit 199 energy levels in the A = 18 – 24 mass region, and a "hole" interaction (CWH) for the upper *sd* shell by varying 20 linear combinations to fit 134 energy levels in the A = 32 – 39 mass region. The least-well-determined linear combinations of matrix elements were fixed at the G-matrix values – the "Sum" value from Table 7 of Ref. [8] and the "12.5p" value from Table I of Ref. [9] for the particle and hole systems, respectively.

The CWP and CWH interactions work well at their respective ends of the *sd* shell, but when they are extrapolated into the middle (A = 25 – 31) they do not quite match and the agreement with experiment worsens [10]. It was soon found that a "universal" hamiltonian (the USD interaction [2]) could be obtained by fitting all of the data simultaneously and by introducing a smooth mass dependence of $A^{-0.3}$ into the matrix elements. The USD interaction was obtained by varying 47 best-determined linear combinations of parameters to fit 447 energy levels in the mass region A = 18 – 39. The 19 least-well-determined linear combinations were fixed to the A = 18 Kuo G-matrix [8]. The mass dependence is an approximate way of taking into account the interpolation between the A = 18 and A = 38 G-matrix. The differences between the fitted two-body matrix elements and the original G-matrix are attributed to many-body effects not included in the G-matrix calculation, such as effective three-body interactions and low-lying core excitations from ^{16}O and ^{40}Ca [2]. Even though the difference between the empirical matrix elements and G-matrix is not large, the effect of the difference builds up quickly with particle (or hole) number, and it is crucial to take into account the empirical adjustments to obtain agreement with spectroscopic data [2, 10].

The GT β decay and electromagnetic properties throughout the *sd* shell are well described by the USD interaction [1, 2], as long as effective operators are used for the GT β-decay and electromagnetic

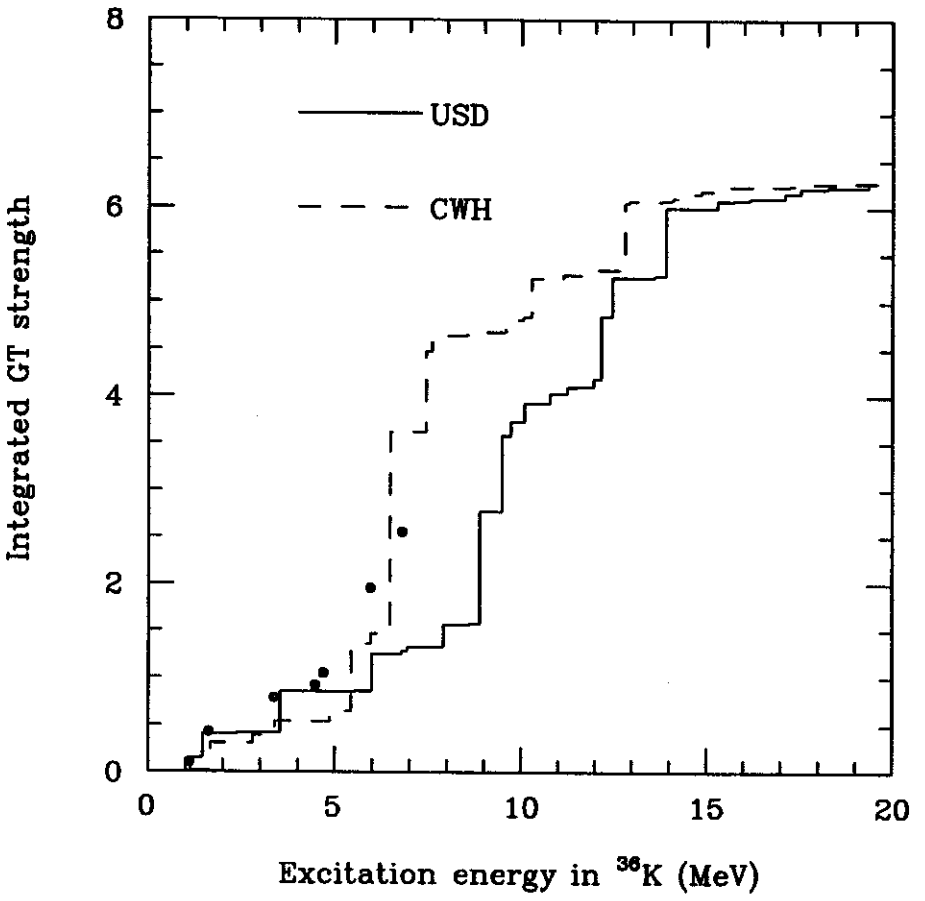

Figure 1: Running sum of the Gamow-Teller strengh for the ^{36}Ca decay; experimental data (points) compared with the calculations.

operators. These effective operators arise from the non-*sd* shell components of the actual wave functions, and the empirical values which are needed to reproduce the experimental data are in qualitative agreement with microscopic calculations which take into account the core-polarization and mesonic exchange contributions [2]. In particular, it is observed that the experimental β-decay strengths are uniformly reduced from the calculated value. The effective $\sigma\tau$ operator which accounts for this "quenching" and which has the mass dependence expected from microscopic calculations [12, 13] mass dependence has the form [1, 2] (ignoring the small orbital and tensor contributions)

$$(\sigma\tau)_{\rm eff} = \left(1 - 0.23\left(\frac{\rm A}{28}\right)^{0.35}\right)(\sigma\tau)_{\rm free}.$$

This approximate effective operator gives a 40% reduction in the middle of the *sd* shell and a 45% reduction in the upper *sd* shell. The full effective GT operator from [1, 2] leads to a 50% reduction in the GT β-decay strength in the upper *sd* shell. The GT strength calculated with both interactions and the full effective GT operator is compared to the experimental data for ^{38}Ca [14], ^{37}Ca (this experiment) and ^{36}Ca (this experiment) in Figures 1 and 2. For the first state in ^{38}Ca and the low-lying states up to 5 MeV in excitation energy (in the K daughter nuclei), the agreement between USD and experiment is

SHELL–MODEL CALCULATIONS FOR THE BINDING ENERGIES OF NUCLEI WITH $A = 86 - 100$ NEAR THE PROTON DRIP LINE

B. Alex Brown and H. Herndl[a]

The nuclear shell model has been highly successful for the calculation of light nuclei with $A < 60$. For most of these isotopes the use of relatively small shell–model spaces is sufficient to calculate observables like binding energies, excitation energies, spectroscopic factors, electromagnetic transition rates, quadrupole moments or beta decay strengths. More massive nuclei require the use of very large model spaces since usually several subshells will be active and the dimensions of wave functions in a subshell with high angular momentum j can be huge. One exception of this general trend is the mass range $86 \leq A \leq 100$ with both N and Z not larger than 50. Here the use of only two subshells, the $2p_{1/2}$– and $1g_{9/2}$–shell, is sufficient to reproduce the spectra of most isotopes. Only few states have significant admixtures of other subshells like the $2p_{3/2}$–, the $1f_{5/2}$– or the $1g_{7/2}$–shell.

In this work we are concerned with the isotopes near the proton drip line which lies close to the $N = Z$ line. We calculate binding energies, excitation energies and beta decay rates of the isotopes in the mass region $86 \leq A \leq 100$. The motivation of this work comes mainly from nuclear astrophysics. In a recent work [1] the rp–process has been extended into this mass region. For the astrophysicist the knowledge of nuclear data like beta decay rates of all isotopes near the proton drip line is essential. We believe that the nuclear shell model can give a good description of these isotopes. With this work we want to provide the nuclear astrophysicist with the necessary nuclear data.

Several effective interactions are available in the $(1g_{9/2}, 2p_{1/2})$ model space. The space covers the region from $38 \leq N, Z \leq 50$ from ^{76}Sr to ^{88}Sr to ^{100}Sn. However, in the lower part of this region the mixing with other single particle levels, especially from the $1f_{5/2}$ and the $2p_{3/2}$ orbitals is very strong, as indicated by the low-lying (deformed) 2^+ states observed in ^{76}Sr and ^{80}Zr [2]. We concluded that the use of only two subshells is justified for isotopes with masses from around 86 and up.

After testing several of the known interactions in the mass range $86 \leq A \leq 99$ where we put special emphasis to isotopes close to the $N = Z$ line, we choose the interaction labeled "T = 0 fit" in Tables 1 and 2 of Ref. [3]. This does not mean that we believe this interaction to be superior to the others. Actually we found similarly satisfactory results with some other interactions. Since we examined isotopes with $N \approx Z$ we found the isospin formalism more appropriate than the proton neutron formalism which was usually employed in all previous compilations. Therefore we transformed the matrix elements of the "T = 0 fit" into isospin formalism and called the interaction SLGT0.

We have calculated the level schemes of all isotopes in the range $86 \leq A \leq 99$ with $N \leq 50$. The nucleus ^{90}Rh has a $J^\pi = 0^+, T = 1$ ground state as do all of the odd–odd $N = Z$ nuclei in our calculations. However, there are also many low–lying $T = 0$ states in ^{90}Rh. (We note that $T = 0$ is the ground state isospin for the odd–odd nuclei with $A = 2 - 30$ and $A = 38$, whereas $T = 1$ is the ground state for $A = 34$ and $A = 42 - 58$. But in all cases the $T = 0$ and $T = 1$ states are close in energy. Above A=58 no experimental information is known. Our calculations are consistent with the general strengthening of the effective $T = 1$ "pairing" interaction over the $T = 0$ "deuteron-like" interaction for the heavy $N = Z$ nuclei.) The nucleus ^{91}Rh has like most $T = 1/2$ isotopes in the region a $9/2^+$ ground state and low lying $7/2^+$ and $1/2^-$ states. The spectrum of ^{92}Pd shows that the typical excitation energy of the first excited 2^+ state in even–even $N = Z$ isotopes in this mass region is at around 900 keV.

The binding energies are important to the nuclear astrophysicist to determine Q–values of proton capture reactions and beta decays. Furthermore the proton drip line depends on the binding energy of all isotopes in the region. Our interaction gives a good account of the relative spacing of the levels. However, since it is an interaction with good isospin, there is no Coulomb interaction. We have not been concerned with the absolute binding energies up to now. In addition to an overall constant, the simplest modifications we can consider is to add terms which are linear and quadratic in the numbers of protons and neutrons. Protons and neutrons are treated separately because of the additional Coulomb interaction between protons. This form is equivalent to taking constant for the two–body Coulomb interaction which may be reasonable given the long–range nature of the Coulomb interaction and the rather small variation in the radial size and mass of the nuclei of interest.

We have thus deduced the binding energy E_B with the five parameter fit

$$E_{\rm tot}({\rm cal}) = -E_B = E_{\rm sm} + a + bn_p + cn_p^2 + dn_n + en_n^2 \qquad (1)$$

with $n_p = Z - 38$ and $n_n = 50 - N$ representing the number of protons and neutron holes in the ($1g_{9/2}$, $2p_{1/2}$) model space. The energy $E_{\rm sm}$ is the energy resulting from the shell–model calculation. The five parameters a to e were determined in a χ^2 fit to the 33 experimentally known binding energies in the range $86 \leq A \leq 100$, $N \leq 50$. The values of the five parameters for the best fit are: a = -806.640 MeV; b = -3.215 MeV; c = 0.139 MeV; d = 14.730 MeV; and e = -0.098 MeV

The constant e is small because the SLGT0 interaction already represents an interaction between neutrons (which was obtained by subtracting a Coulomb interaction from a fit to the $N = 50$ isotones [3]). The difference between b and d is related to the Coulomb energy of the valence protons with the core protons, and the term c represents the effective two–body Coulomb interaction between valence protons. We have included the experimental binding energies of 33 nuclei in the region of interest to determined the parameters. The experimental and theoretical binding energies with errors are given in Table 1. It can be seen that the experimental binding energies are reproduced satisfactorily. The rms deviation of the 33 masses is 131 keV.

We then used eq. (1) to calculate all neutron-deficient isotopes up to the proton drip line. The comparison of our binding energies with the extrapolated energies from Refs. [4, 5] (extrapolation from the systematic trend) shows that our values lie well within the error bars in almost all cases. For some isotopes like ^{98}Cd or ^{92}Rh the agreement is almost perfect. In the case of ^{100}Sn, our binding energy is 0.4 ± 0.4 MeV smaller than the Audi-Wapstra extrapolation and 1.3 ± 0.9 smaller than a recent mass measurement [6] (the errors are from the extrapolation or experiment). Some isotopes (i.e. ^{88}Pd, ^{89}Pd, ^{92}Cd, ^{93}Cd and ^{98}Sn) are bound against one proton but unbound against two proton decay.

Recent experiments on the stability of the most neutron-deficient nuclei in this region [7, 8] are sensitive to those whose lifetime is greater than a few hundred nanoseconds. In addition to the binding energy, ones needs to consider the barrier penetration factor for the proton decay of the unbound nuclei. The dominant mode of decay for $Z > 44$ should be by the emission of an $g_{9/2}$ ($\ell = 4$), proton. Using the Wigner single-particle width (with a spectroscopic factor of unity) plus a penetrability factor obtained from Coulomb wave functions [9] starting at $R = 5.8$ fm, we estimate that the states which are unbound by about 1 MeV could have a lifetime in the few hundred nanosecond range. Those nuclei which could have lifetimes of a few hundred nanosecond or greater start at ^{94}Sn (Z=50), ^{97}In (Z=49), ^{89}Cd (Z=48), ^{92}Ag (Z=47), ^{87}Pd (Z=46) and ^{88}Rh (Z=45). The most neutron–deficient nuclei observed experimentally [7, 8] are ^{100}Sn (Z=50), ^{98}In (Z=49), ^{96}Cd (Z=48), ^{94}Ag (Z=47), ^{91}Pd (Z=46) and ^{89}Rh (Z=45), with a tentative

Table 1: Experimental and calculated binding energies of 33 neutron-deficient isotopes with experimental error σ and the deviation of theory and experiment $\delta E = E_B(\text{exp}) - E_B(\text{cal})$. The experimental data are taken from Refs. [4, 5].

N	Z	nucleus	E_B(exp)	σ	E_B(cal)	δE
50	38	^{88}Sr	768.464	0.002	768.472	−0.008
	39	^{89}Y	775.537	0.002	775.525	0.012
	40	^{90}Zr	783.894	0.002	783.868	0.026
	41	^{91}Nb	789.053	0.003	789.119	−0.066
	42	^{92}Mo	796.509	0.004	796.534	−0.025
	43	^{93}Tc	800.596	0.004	800.670	−0.074
	44	^{94}Ru	806.843	0.013	806.903	−0.060
	45	^{95}Rh	809.900	0.150	809.926	−0.026
	46	^{96}Pd	815.030	0.150	815.020	0.010
49	38	^{87}Sr	757.352	0.002	757.303	0.049
	39	^{88}Y	764.060	0.003	764.111	−0.051
	40	^{89}Zr	771.923	0.003	771.854	0.069
	41	^{90}Nb	777.001	0.005	776.990	0.011
	42	^{91}Mo	783.837	0.012	783.784	0.053
	43	^{92}Tc	787.857	0.026	787.809	0.048
	44	^{93}Ru	793.480	0.090	793.374	0.106
48	38	^{86}Sr	748.924	0.002	748.740	0.184
	39	^{87}Y	754.708	0.003	754.849	−0.141
	40	^{88}Zr	762.607	0.010	762.437	0.170
	41	^{89}Nb	766.850	0.040	766.904	−0.054
	42	^{90}Mo	773.730	0.006	773.587	0.143
	43	^{91}Tc	776.830	0.200	776.897	−0.067
47	39	^{86}Y	742.901	0.014	−743.260	−0.359
	40	^{87}Zr	750.260	0.008	750.234	0.026
	42	^{89}Mo	760.493	0.015	760.581	−0.088
	43	^{90}Tc	763.988	0.240	763.774	0.214
	44	^{91}Ru	768.650	0.500	768.498	0.152
46	40	^{86}Zr	740.650	0.030	740.626	0.024
	41	^{87}Nb	744.310	0.060	744.326	−0.016
	42	^{88}Mo	750.119	0.020	750.167	−0.048
	43	^{89}Tc	752.200	0.210	752.577	−0.377
45	41	^{86}Nb	731.890	0.090	731.717	0.173
	42	^{87}Mo	737.040	0.220	736.860	0.180

indication [8] of ^{99}Sn and ^{93}Ag. It will take a new generation of experiments to fully explore the drip-line nuclei and their decay modes in this mass region. As mentioned above there are candidates for two-proton emission which may eventually supplement those being searched for in lighter nuclei [10].

a. Institut f. Kernphysik, TU Wein, Wien, Austria

References

1. H. Schatz, A. Aprahamian, J. Görres, M. Wiescher, F.-K. Thielemann, T. Rauscher, K.-L. Kratz, B. Pfeiffer, P. Möller, H. Herndl, B.A. Brown, to be published in Physics Reports.
2. C.J. Lister, P.J. Ennis, A.A. Chishti, B.J. Varley, W. Gelletly, H.G. Price and A.N. James, Phys. Rev. C42 (1990) R1191.
3. F.J.D. Serduke, R.D. Lawson and D.H. Gloeckner, Nucl. Phys. A256 (1976) 45.
4. G. Audi and A.H. Wapstra, Nucl. Phys. A565 (1993) 1.
5. G. Audi and A.H. Wapstra, Nucl. Phys. A595 (1995) 409.
6. M. Chartier et al., Phys. Rev. Lett. 77, 9 (1996).
7. M. Hensheck, et al., Phys. Rev. C50 (1994) 2219.
8. K. Rykaczewski, et al.,Phys. Rev. C52 (1995) R2310.
9. A. R. Barnett, Comput. Phys. Commun. 27 (1982) 147.
10. B. A. Brown, Phys. Rev. C43 (1991) R1513; C44 (1991) 924.

SHELL–MODEL CALCULATIONS FOR THE HALF LIVES OF NUCLEI WITH $A = 86 - 100$ NEAR THE PROTON DRIP LINE

B. Alex Brown and H. Herndl[a]

Using the SLGT0 interaction discussed previously, we have calculated the half lives of all isotopes in the region just below ^{100}Sn Most of the nuclei decay by Gamow–Teller transitions. In a few cases Fermi transitions have to be taken into account. The decay of the $J = 0, T = 1$ ground states of odd–odd $N = Z$ nuclei is dominated by the Fermi transition to its analog state. Fermi transitions also occur for the decay of isotopes with $Z = N + 1$ to their mirror nuclei.

The partial half–life is related to the Fermi and Gamow-Teller matrix elements by [1] $(f_v + f_{EC})B(F) + (f_a + f_{EC})B(GT) = 6177s/t_{1/2}$. The Gamow–Teller and Fermi transition strengths B(GT) and B(F) are obtained from our shell–model wave functions. The vector and axial vector phase–space factors f_v and f_a are calculated with the formulae given in Ref. [2] and the electron–capture phase–space factors f_{EC} are based on the Tables of Ref. [3].

We first calculated the Gamow–Teller matrix elements with the free–nucleon operator (see [1]). In Table 1 the calculated half lives are compared with the experiment.

Several of the states in the Table are not the ground states. They are marked by an asterisk. Most odd isotopes have a $9/2^+$ ground state and a $1/2^-$ isomeric state. In two cases the half life of the $1/2^-$ state is not purely given by the beta decay but also by an isomeric E3 transition to a low lying $7/2^+$ state. For the $1/2^-$ states in ^{91}Mo and ^{93}Ru the ratio of beta decay is given by 49.9% and 78%, respectively. In the Table we give the experimental partial half lives, calculated from the total half lives and the branchings.

With one exception the data agree within one order of magnitude. Previous compilations of Gamow–Teller strengths have reported a general trend that the calculated values overestimate the experimental data. Therefore average quenching factors were introduced; $(\sigma\tau)_{eff} = (1 - q)(\sigma\tau)_{free}$. This factor was $q = 0.24 \pm 0.03$ in Ref. [1] for the sd–shell or $q = 0.21$ in Ref. [4] for the lower fp–shell. In our compilation, however, this general trend can not be observed. Both overestimation and underestimation of the experimental data occurs.

If one looks into the orbital dependence of the Gamow–Teller matrix elements, the decay from the $9/2^+$ states are dominated by $g_{9/2}$ whereas the decay from the $1/2^-$ is determined by a cancellation between the $g_{9/2}$ and the $p_{1/2}$ contributions. Thus, although the agreement between experiment and theory cannot be improved by the introduction of an overall quenching factor, it turns out that the agreement can be greatly improved by the introduction of an orbit-dependent quenching factor, namely, $q = 0.40$ for $g_{9/2}$ and $q = 0$ for $p_{1/2}$. The results with the effective operator are shown in Table 1. The improvement is good except for the decay of some of the 0^+ ground states whose agreement between theory and experiment becomes worse in a few cases.

We can speculate on the qualitative origin of this orbit–dependent quenching. The rather large value required for $g_{9/2}$ is consistent with the combined effect of the first–order mixing with the $g_{7/2}$–$g_{9/2}$ particle–hole giant Gamow–Teller resonance which is not explicitly included in our model space, together with the higher-order effects responsible for the sd–shell and fp–shell quenching mentioned above. The $p_{1/2}$ orbit is special with regard to quenching — it is well know that the first–order effects due to mixing with the $p_{3/2}$ vanish in the limit of a zero–range interaction [5], and this explains why all nuclei with $p_{1/2}$ ground states have magnetic moments close to their Schmidt value.

Table 1: Experimental and calculated half lives. States marked by an asterisk are not the ground states. Explanation in the text.

nucleus	J_i^π	T_i	$t_{1/2}$(exp)	$t_{1/2}$(free)	$t_{1/2}$(eff.)
^{86}Zr	0^+	3	5.94×10^4	62.3×10^4	164.5×10^4
^{87}Zr	$9/2^+$	7/2	6.05×10^3	2.13×10^3	6.08×10^3
^{88}Zr	0^+	4	7.21×10^6	79.6×10^6	19.2×10^6
^{87}Nb	$1/2^-$	5/2	2.22×10^2	5.78×10^2	3.09×10^2
	$9/2^{+*}$	5/2	15.6×10^1	6.80×10^1	18.1×10^1
^{88}Nb	8^+	3	8.70×10^2	1.49×10^2	6.95×10^2
^{89}Nb	$9/2^+$	7/2	68.4×10^2	5.94×10^2	16.7×10^2
	$1/2^{-*}$	7/2	4.25×10^3	11.0×10^3	3.87×10^3
^{90}Nb	8^+	4	52.6×10^3	8.46×10^3	26.8×10^3
^{86}Mo	0^+	1	1.96×10^1	2.06×10^1	7.40×10^1
^{87}Mo	$9/2^+$	3/2	1.34×10^1	1.09×10^1	3.09×10^1
^{88}Mo	0^+	2	4.8×10^2	11.2×10^2	74.5×10^2
^{89}Mo	$9/2^+$	5/2	12.3×10^1	4.56×10^1	14.0×10^1
^{90}Mo	0^+	3	2.04×10^4	7.75×10^4	59.9×10^4
^{91}Mo	$9/2^+$	7/2	9.29×10^2	3.12×10^2	9.03×10^2
	$1/2^{-*}$	7/2	1.30×10^2	17.0×10^2	2.41×10^2
^{89}Tc	$9/2^+$	3/2	12.8	4.5	12.9
	$1/2^{-*}$	3/2	12.9	42.1	113.1
^{90}Tc	2^+	2	8.70	11.3	32.8
	4^{-*}	2	4.92×10^1	2.41×10^1	5.20×10^1
^{91}Tc	$9/2^+$	5/2	18.8×10^1	4.49×10^1	12.6×10^1
	$1/2^{-*}$	5/2	1.98×10^2	2.23×10^2	1.94×10^2
^{92}Tc	8^+	3	2.54×10^2	1.02×10^2	2.99×10^2
^{90}Ru	0^+	1	13.0	12.5	41.5
^{91}Ru	$9/2^+$	3/2	9.0	4.33	12.3
	$1/2^{-*}$	3/2	7.6	21.2	9.47
^{92}Ru	0^+	2	2.19×10^3	4.53×10^3	2.11×10^3
^{93}Ru	$9/2^+$	5/2	5.97×10^1	2.17×10^1	6.23×10^1
	$1/2^{-*}$	5/2	1.38×10^1	10.6×10^1	2.71×10^1
^{94}Rh	8^+	2	2.58×10^1	1.13×10^1	3.17×10^1
	4^{+*}	2	7.06×10^1	3.82×10^1	11.4×10^1
^{94}Pd	0^+	1	9.0	9.65	30.1
^{95}Pd	$21/2^{+*}$	3/2	13.3	8.47	24.7
^{94}Ag	9^{+*}	0	42.0×10^{-2}	9.40×10^{-2}	26.5×10^{-2}
^{95}Ag	$9/2^+$	1/2	2.0	0.67	1.85
^{96}Ag	8^+	1	5.1	1.86	5.32

a. Institut f. Kernphysik, TU Wein, Wien, Austria

References

1. B.A. Brown and B.H. Wildenthal, Atomic Data and Nuclear Data Tables 33 (1985) 347.
2. B.H. Wilkinson and B.E.F. Macefield, Nucl. Phys. A232 (1974) 58.
3. H. Behrens and J. Janecke, in Landolt and Bornstein, Numerical Data and Functional Relationships in Science and Technology, New Series, editor in chief K.–H. Hellwege, Group I: *Nuclear Physics and Technology*, Vol. 4, edited by H. Schopper (Springer–Verlag, New York/Berlin, 1969)
4. W.A. Richter, M.G. Van der Merwe, R.E. Julies and B.A. Brown, Nucl. Phys. A577 (1994) 585.
5. B. Castel and I.S. Towner, Modern Theories of Nuclear Moments, Clarendon Press, Oxford, 1990.

INELASTIC ELECTRON SCATTERING AS AN INDICATOR OF CLUSTERING

S. Karataglidis, B. A. Brown, K. Amos[a], and P. J. Dortmans[a]

While the shell model is the most fundamental of nuclear structure models, states in light nuclei also have been described successfully in terms of clusters. Indeed, Wildemuth and Tang [1] have shown a correspondence between the cluster and shell models, the clusters arising naturally as correlations out of the shell model Hamiltonian. For light nuclei, the cluster model reduces the many-body problem to a few-body one, with interactions occurring between the clusters. These interactions involve particle exchanges, since the nucleons may still be considered somewhat freely moving, with their motion not strictly confined to the clusters themselves. Such is the relation of the cluster model to the shell model. For a realistic shell model then, one may expect some evidence of clustering in the wave functions for those systems in which the cluster model is valid.

A good place to look for this behavior is in the ^{6}Li and ^{7}Li nuclei. Both of these have been described successfully in terms of clusters [2], as $\alpha + d$ in the case of ^{6}Li (or as $\alpha + p + n$ in a three-body description [3]), and $\alpha + t$ for ^{7}Li, although other two-cluster configurations are possible [2]. The simple $0\hbar\omega$ shell model descriptions of these nuclei automatically contain such clustering: the $0s$-shell inert core is the α particle, while the valence nucleons in the $0p$-shell naturally form the other cluster. More recently, large space multi-$\hbar\omega$ shell models have been constructed for these nuclei [4]. Such are required if a shell model approach is to model cluster effects realistically [5].

This clustering behavior in the shell model wave functions can be illustrated by considering the $E2$ transitions to the low-lying excited states in both ^{6}Li, to the $3^+;0$ (2.186 MeV) state, and ^{7}Li, to the $\frac{1}{2}^-$ (0.478 MeV) and the $\frac{7}{2}^-$ (4.63 MeV) states. The shell model wave functions for both nuclei were constructed in complete $0\hbar\omega$, $(0+2)\hbar\omega$, and $(0+2+4)\hbar\omega$ model spaces using the Cohen and Kurath $(6-16)$2BME (CK) [6], the MK3W [7], and the Zheng interactions [4], respectively. For comparison, the Zheng interaction was also used to construct wave functions in the $0\hbar\omega$ and $(0+2)\hbar\omega$ spaces. All shell model calculations were performed using the code OXBASH [8]. The B($E2$) values, calculated using harmonic oscillator wave functions determined from analyses of elastic electron scattering form factors [9], for those $E2$ transitions are compared in Table 1 to the experimental values [10,11]. The results obtained using the multi-$\hbar\omega$ shell

Table 1: B(E2$\downarrow$) values (in units of e^2 fm^4) for the transitions in ^{6,7}Li as listed.

Nucleus	Transition	$0\hbar\omega$		$(0+2)\hbar\omega$		$(0+2+4)\hbar\omega$	Expt. [8]
		CK	Zheng	MK3W	Zheng		
^{6}Li	$3^+;0 \rightarrow$ g.s.	2.65		4.31		4.07	9.3 ± 2.1
^{7}Li	$\frac{1}{2}^- \rightarrow$ g.s.	3.04	2.51	8.00	6.21	7.23	16.4 ± 1.0
	$\frac{7}{2}^- \rightarrow$ g.s.	1.04	1.30	3.30	2.88	3.32	$3.50, 7.5 \pm 0.8$[a)]

a) Ref. [11].

model wave functions are closer in agreement with experiment than the results obtained using the $0\hbar\omega$ wave functions. Yet in all cases, that level of agreement is not good, with the calculations underpredicting the measured values by at least a factor of two. This indicates that the shell model wave functions do not exhibit clustering behavior, which is expected to manifest itself at small momentum transfer. The

exception is the transition to the $\frac{7}{2}^-$ state in ^{7}Li, for which the value obtained from the γ-decay width [10] is in agreement with the value obtained from the MK3W and $(0+2+4)\hbar\omega$ shell model calculations. However, that measured value quoted in the compilation [10] is not referenced, and so one must look to an alternative analysis by which the two measurements may be compared.

We obtained the B($E2$) as a function of momentum transfer from the calculated longitudinal electron scattering form factors [9] using the transformation of Brown, Radhi, and Wildenthal [12]. That transformation removes most of the dependence on momentum transfer from the form factor; the measured B($E2$) value is compared to the $q = 0$ intercept. This is illustrated in Fig. 1, wherein the longitudinal inelastic electron scattering form factor to the $3^+;0$ (2.186 MeV) state in ^{6}Li and the associated B($E2, q$) are displayed in (a) and (b) respectively. The results obtained using the $(0+2+4)\hbar\omega$, $(0+2)\hbar\omega$, and $0\hbar\omega$ wave

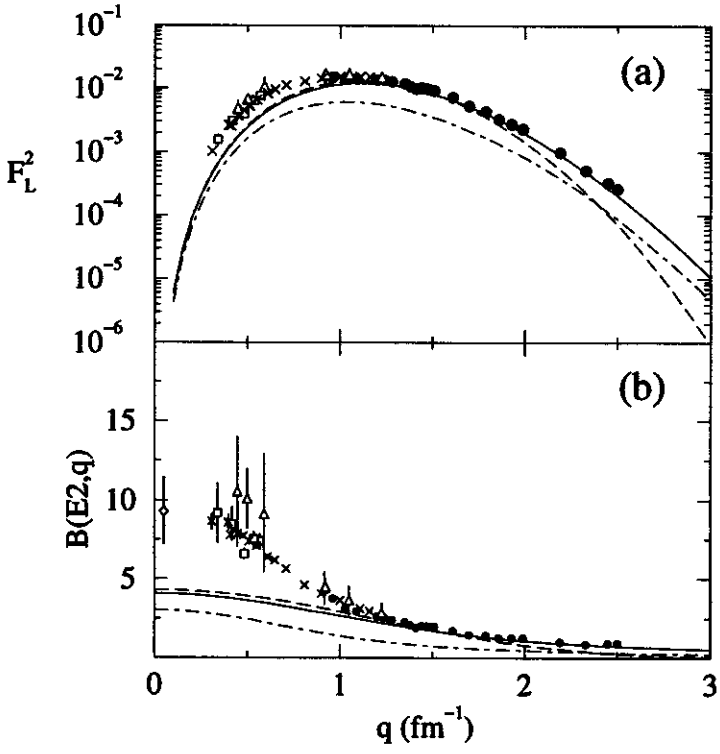

Figure 1: Longitudinal inelastic electron scattering form factor to the $3^+;0$ (2.186 MeV) state in ^{6}Li (a), and the B(E2$\downarrow$,q) value, in units of e^2 fm^4, as obtained from the form factor (b). The data of Bergstrom *et al.* [13] (circles), Yen *et al.* [14] (squares), Bergstrom and Tomusiak [15] (crosses), and Hutcheon and Caplan [16] (triangles) are compared to the results of the calculations made using the $(0+2+4)\hbar\omega$ wave functions (solid line), the MK3W wave functions (dashed line), and the CK wave functions (dot-dashed line). The B(E2$\downarrow$) value from the associated γ–decay rate [10] is displayed by the diamond data point in (b).

functions are displayed by the solid, dashed, and dot-dashed lines respectively. They are compared to the data of Bergstrom *et al.* [13] (circles), Yen *et al.* [14] (squares), Bergstrom and Tomusiak [15] (crosses), and Hutcheon and Caplan [16] (triangles). The form factor illustrates the discrepancy in the predictions of the B($E2$) value. For the multi-$\hbar\omega$ models, there is agreement with data above 1 fm^{-1}. However, all models fall below the data below 1 fm^{-1}. The B($E2, q$), displayed in Fig. 1(b), shows that discrepancy more clearly,

with the data converging on the measured value (indicated by the diamond data point), and the results of the calculations falling well below that value.

The B($E2, q$) obtained from the longitudinal inelastic electron scattering form factor to the $\frac{7}{2}^-$ (4.63 MeV) state in ^{7}Li is displayed in Fig. 2(a). There is some doubt on the measured B(E2$\downarrow$) for this

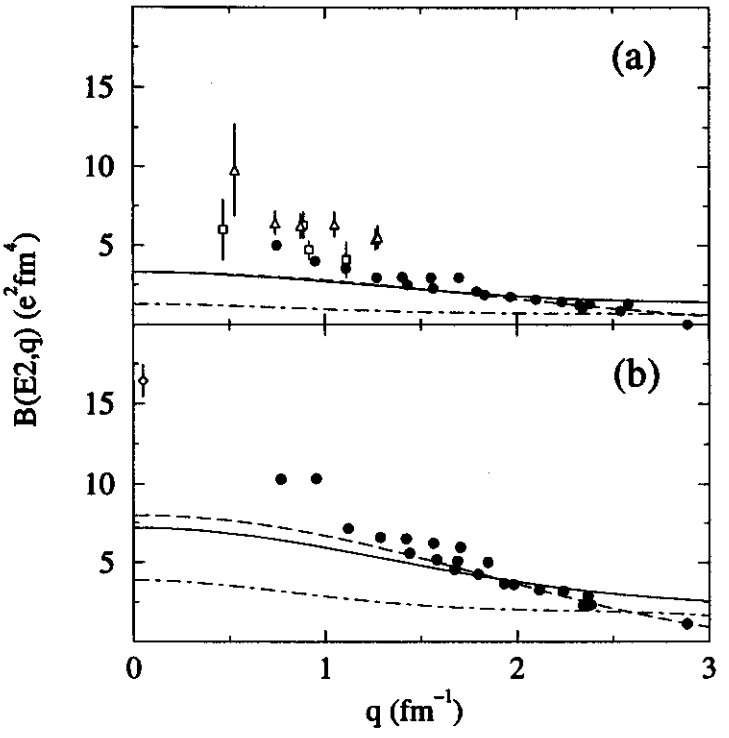

Figure 2: B(E2$\downarrow$,q) for the $\frac{7}{2}^-$ (4.63 MeV) (a) and the $\frac{1}{2}^-$ (0.478 MeV) (b) states in ^{7}Li. The data of Lichtenstadt *et al.* [11] (circles), Hutcheon and Caplan [16] (squares), and Bernheim and Bishop [17] (triangles) are compared to our results obtained using the various shell models. The measured B(E2$\downarrow$) value for the $\frac{1}{2}^-$ state in ^{7}Li [10], as determined from the γ–decay rate, is given by the diamond data point.

transition. From the quoted γ–decay rate this is 3.50 e^2 fm^4 [10], however, the source of that measurement is not given in the compilation. The value obtained from an analysis of the longitudinal inelastic electron scattering form factor is 7.5 ± 0.8 e^2 fm^4 [11]. Therein, the B(E2) value for the decay of the $\frac{7}{2}^-$ state is related to that for the $\frac{1}{2}^-$ state, which is well determined. The values obtained from the various shell models are listed in Table 1. Our results obtained from the $(0+2)\hbar\omega$ and $(0+2+4)\hbar\omega$ shell models lie very close to the value obtained from the γ–decay. The data of Lichtenstadt *et al.* [11] (circles), Hutcheon and Caplan [16] (squares), and Bernheim and Bishop [17] (triangles) are compared to our results obtained using the various shell models. A similar discrepancy of our results with data to those observed for the $3^+;0$ state in ^{6}Li [Fig. 1(b)] and the $\frac{1}{2}^-$ state in ^{7}Li, displayed in Fig. 2(b), is now also observed, with the data suggesting a B(E2) value of around 7 or 8 e^2 fm^4. More accurate measurements of the form factor for the $\frac{7}{2}^-$ state are necessary below $q = 0.5$ fm^{-1} in order to resolve the remaining discrepancy with the quoted γ–decay rate.

From these results, and also of analyses of the electron and proton scattering observables [9], the shell model wave functions, obtained in the $(0+2+4)\hbar\omega$ model space, do not exhibit the correlations necessary to define the clustering of the wave functions.

a. School of Physics, University of Melbourne, Parkville, Vic. 3052, Australia.

References

1. K. Wildemuth and Y. C. Tang, *A Unified Theory of the Nucleus* (Academic Press, 1977).
2. K. Langanke, Adv. Nucl. Phys. 21, 85 (1994), and references cited therein.
3. N. W. Schellingerhout, L. P. Kok, S. A. Coon, and R. M. Adam, Phys. Rev. C 48, 2714 (1993).
4. D. C. Zheng, B. R. Barrett, J. P. Vary, W. C. Haxton, and C.-L. Song, Phys. Rev. C 52, 2488 (1995).
5. A. Arima, H. Horiuchi, K. Kubodera, and N. Takigawa, Adv. Nucl. Phys. 5, 345 (1972).
6. S. Cohen and D. Kurath, Nucl. Phys. 73, 1 (1965).
7. E. K. Warburton and D. J. Millener, Phys. Rev C 39, 1120 (1989).
8. OXBASH-MSU (the Oxford-Buenos-Aries-Michigan State University shell model code), A. Etchegoyen, W. D. M. Rae, and N. S. Godwin (MSU version by B. A. Brown, 1986); B. A. Brown, A. Etchegoyen, and W, D. M Rae, MUSCL Report No. 524, 1986 (unpublished).
9. S. Karataglidis, B. A. Brown, K. Amos, and P. J. Dortmans, Phys. Rev. C, in press (1997).
10. F. Ajzenberg-Selove, Nucl. Phys. A490, 1 (1988).
11. J. Lichtenstadt, J. Alster, M. A. Moinester, J. Dubach, R. S. Hicks, G. A. Peterson, and S. Kowalski, Phys. Lett. B 244, 173 (1990).
12. B. A. Brown, R. Radhi, and B. H. Wildenthal, Phys. Rep. 101, 313 (1983).
13. J. C. Bergstrom, U. Deutschmann, and R. Neuhausen, Nucl. Phys. A327, 439 (1979).
14. R. Yen, L. S. Cardman, D. Kalinsky, J. R. Legg, and C. K. Bockelman, Nucl. Phys. A235, 135 (1974).
15. J. C. Bergstrom and E. L. Tomusiak, Nucl. Phys. A262, 196 (1976).
16. R. M. Hutcheon and H. S. Caplan, Nucl. Phys. A127, 417 (1969).
17. M. Bernheim and G. R. Bishop, Phys. Lett. 5, 294 (1963).

CHARGED PION PHOTOPRODUCTION AS A PROBE OF HALO NUCLEI

S. Karataglidis, C. Bennhold[a], and L. Tiator[b]

Much information on the momentum distributions of halo nucleons in halo nuclei has been gained from heavy ion collisions. However, in those violent collisions only the external part of the halo may be probed [1,2], providing no detail of the part of the halo wave function that may exist in the interior of the core. Studying the external part only is of itself interesting, coming solely from the long tail of the radial wave functions. Halos are characterised by low angular momenta [3], with $l = 0$ most favored, as the centrifugal barrier confines the nucleons with increasing angular momenta. As the s–wave radial wave functions peak at the origin, one also seeks a way of probing those halo single particle wave functions at small distances. This has the benefit of also studying the interaction of the halo with the core. Halo states may be formed by single charge exchange reactions on light stable nuclei, and hence such reactions may provide a means for studying those wave functions as a whole.

Single charge exchange reactions fall into two broad classes: those mediated by the strong interaction [(p,n), (n,p), or $(\pi^{\pm},\pi^{0})$] and those mediated by the electromagnetic interaction [$(\gamma,\pi^{\pm})$]. The latter are favored for the study of halo states as they are soft electromagnetic reactions, and can largely preserve the momenta of the halo nucleons. The purpose of this investigation is to study the feasibility of pion photoproduction experiments leading to halo nuclear states, and if the experiments are sensitive to the details of the momentum wave functions of the halo nucleons. Several reactions are possible: e.g. $^{6}\mathrm{Li}(\gamma,\pi^{+})^{6}\mathrm{He}_{g.s.}$, $^{11}\mathrm{B}(\gamma,\pi^{+})^{11}\mathrm{Be}$, $^{15}\mathrm{N}(\gamma,\pi^{+})^{15}\mathrm{C}$, and $^{17}\mathrm{O}(\gamma,\pi^{-})^{17}\mathrm{F}$. Ideally, one would also require complementary data from nucleon or pion charge exchange reactions leading to the same halo states. Together with the photopion data, they would provide the most sensitive tests available for the halo wave functions.

Our starting point is to construct the target and halo nuclear wave functions from the shell model, from which the one-body density matrix elements (OBDME) for the transition are obtained. The OBDME are then used in calculations of the pion photoproduction differential cross sections in either a plane wave (PWIA) or distorted wave (DWIA) impulse approximation. The formalism of Tiator and Wright [4] is used to obtain the cross sections in both models. As an example, we present calculations for the $^{11}\mathrm{B}(\gamma,\pi^{+})^{11}\mathrm{Be}$ cross section at $E_{\gamma} = 200$ MeV.

The ^{11}Be nucleus presents a well-known problem for the shell model. Its ground and first excited states are $\frac{1}{2}^{+}$; $\frac{3}{2}$ and $\frac{1}{2}^{-}$ (0.32 MeV) [5], respectively. Thus the ground state is a $1\hbar\omega$ state while the first $0\hbar\omega$ state is the 0.32 MeV state. Any shell model description of the nucleus should reproduce this inversion. We have performed a complete $(0+1)\hbar\omega$ shell model calculation using the WBP interaction of Warburton and Brown [6]. The inversion is reproduced in this model, with the $\frac{1}{2}^{-}$ $(0\hbar\omega)$ state lying at 0.071 MeV above the $\frac{1}{2}^{+}$ $(1\hbar\omega)$ ground state. The ^{11}Be ground state in this model is $76.83\%\left|\left(1s_{\frac{1}{2}}\right)^{1}\times{}^{10}\mathrm{Be}(0^{+})\right\rangle + 23.17\%\left|\left(0d_{\frac{5}{2}}\right)^{1}\times{}^{10}\mathrm{Be}(2^{+})\right\rangle$, which predicts the dominance of the s–wave halo [3]. However, it should be noted that in the simple ^{10}Be+n model, the halo neutron is assumed to be purely in a $1s_{\frac{1}{2}}$ orbit [3]. The ^{11}B ground state was calculated in the same model and is purely $0p$-shell, with a ground state of $\frac{3}{2}^{-}$; $\frac{1}{2}$.

The PWIA or DWIA amplitudes are constructed from the nonrelativistic Blomqvist-Laget (BL) operator [7] for the elementary pion photoproduction process. The BL operator in its original form is non-unitary, but a unitarized version is now available. We consider results using both forms. The construction of the amplitude for the nuclear case involves an integral over the initial and final momenta of the initial and final nucleon wave functions along with the outgoing pion wave function, viz. Eqs. (11) and (12) in [4]. That dependence on the final state single nucleon wave function is measured in experiment. In the case where the final state is a halo nucleus, it gives a measure of the momentum distribution of the final state halo nucleon in those transitions which lead to its formation. Hence a pure transition is favored, such as $^{17}O(\gamma,\pi^-)^{17}F^*$ (0.495 MeV), as the shell model description of the final state is a pure $1s_{\frac{1}{2}}$ proton halo. The single particle wave functions are chosen to be of harmonic oscillator (HO) form, except for those orbits which correspond to the halo nucleons. In that case, single particle wave functions of Woods-Saxon (WS) form are employed, to reproduce the extended radial distribution associated with halos, with the binding energy of the wave function being chosen as the separation energy of the halo nucleon. For ^{11}Be, that separation energy is 0.5 MeV [5], while the oscillator length for the HO wave functions was set to 1.67 fm.

Fig. 1 displays the results of our calculations of the $^{11}B(\gamma,\pi^+)^{11}Be_{gs}$ cross section at a photon energy of 200 MeV. Therein, the results of our calculations using the HO and WS forms are displayed in

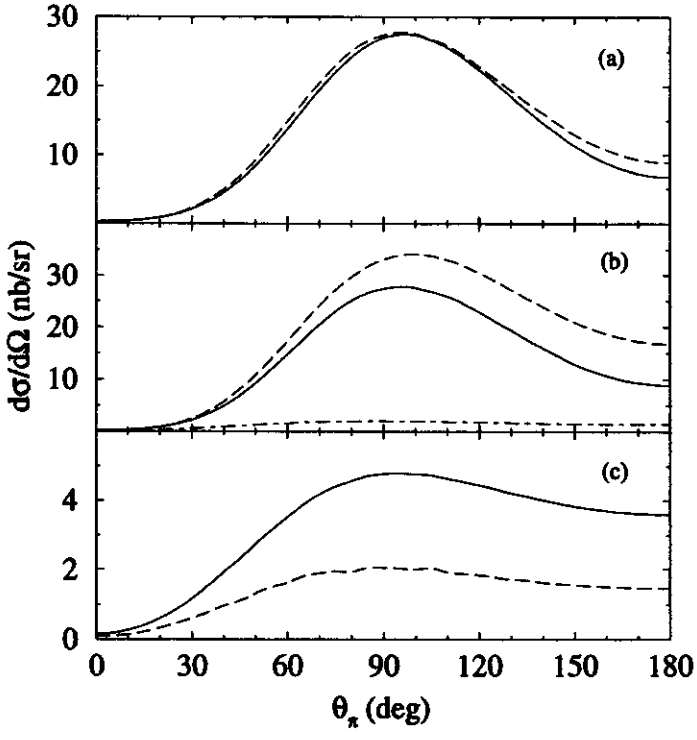

Figure 1: Differential cross section for the $^{11}B(\gamma,\pi^+)^{11}Be_{gs}$ reaction. (a) Results of our calculations using single particle wave functions of HO (solid line) and WS (dashed line) forms as described in the text; (b) The $0p \rightarrow 0d$ (dashed line) and $0p \rightarrow 1s$ (dot-dashed line) transitions as compared to the total cross section (solid line); (c) The $0p \rightarrow 1s$ component of the cross section as calculated using HO (solid line) and WS (dashed line) forms.

Fig.1(a) by the solid and dashed lines respectively. The results using both forms of the BL operator are very similar; only those using the nonunitary form are displayed. The effect of using the extended WS wave functions for the halo orbits is clearly evident; the effect is to increase the cross section at large angles by $\sim 30\%$. That increase is due to the destructive interference between the $0p \rightarrow 0d$ and $0p \rightarrow 1s$ components of the cross section as displayed in Fig. 1(b). While the $0p \rightarrow 1s$ transition is much smaller than the dominant $0p \rightarrow 0d$ one, the change in that transition brought by the use of the WS wave function, illustrated in Fig. 1(c), is measureable by its interference with the other transition.

However, the measurement of the ground state transition is concomitant with the ability to separate out the ground state of ^{11}Be with the 0.32 MeV excited state in the experiment. That would require very high resolution, which may only now be achievable by tagging experiments at TUNL [8]. The differential cross section to the excited state is also of interest, as that is an example of a $0p$–shell halo, and should also be measured. Fig. 2 shows the ground and excited state cross sections, displayed by the dashed and solid lines, respectively. Note that the excited state calculation assumed no halo in this case. The excited state cross section is predicted to be at least a factor of 15 greater than the ground

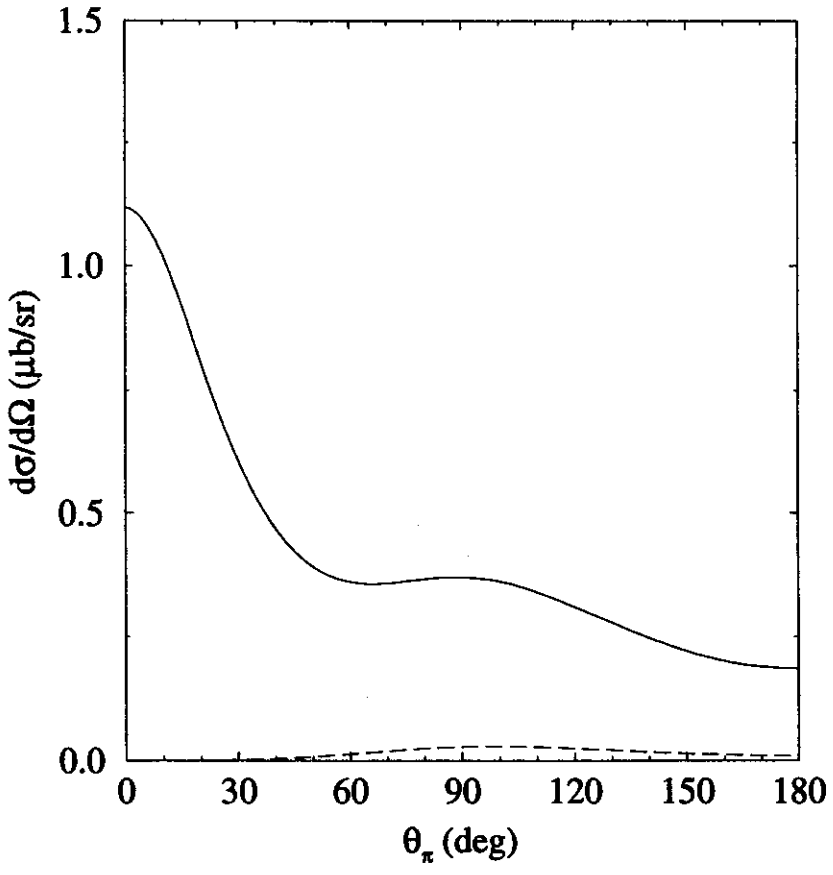

Figure 2: Differential cross section for ^{11}B$(\gamma, \pi^+)^{11}$Be leading to the ground (dashed line) and 0.32 MeV excited (dashed line) states.

state cross section. Hence, an accurate measurement of the ground and excited state cross sections for the

$^{11}B(\gamma,\pi^+)^{11}Be$ reaction represents a difficult challenge for experimenters.

We are also pursuing calculations of the other reactions mentioned above. The calculation of the $^{11}B(\gamma,\pi^+)^{11}Be^*$ (0.32 MeV) assuming a halo is of interest to see what effect the halo has on the relative cross section. The $^6Li(\gamma,\pi^+)^6He_{g.s.}$ reaction is also of particular interest. First, there are data available for this cross section [9]. Second, the ^6He ground state is the isobaric analogue of the $0^+;1$ (3.56 MeV) state in ^6Li. As such, the $^6Li(\gamma,\pi^+)^6He_{g.s.}$ reaction is related to inelastic scattering from ^6Li leading to the $0^+;1$ state. That correspondence allows for a strict assessment of the nuclear wave functions, allowing for a more accurate prediction of the cross section.

a. Department of Physics, Center for Nuclear Studies, The George Washington University, Washington, D.C. 20052
b. Institut für Kernphysik, Johannes Gutenburg-Universität, D-55099 Mainz, Germany

References

1. P. G. Hansen, Phys. Rev. Lett. 77, 1016 (1996).
2. H. Esbensen, Phys. Rev. C 53, 2007 (1996).
3. K. Riisaga, Rev. Mod. Phys. 66, 1105 (1994).
4. L. Tiator and L. E. Wright, Phys. Rev. C 30, 989 (1984).
5. F. Ajzenberg-Selove, Nucl. Phys. A506, 1 (1990).
6. E. K. Warburton and B. A. Brown, Phys. Rev. C 46, 923 (1992).
7. K. I. Blomqvist and J. M. Laget, Nucl. Phys. A280, 405 (1977).
8. E. C. Schreiber *et al.*, Bull. Am. Phys. Soc. 42, 993 (1997).
9. J. Shaw *et al.*, Phys. Rev. C 43, 1800 (1991).

INTERACTING BOSON-FERMION APPROXIMATION CALCULATIONS FOR PRASEODYMIUM NUCLEI

W.A. Olivier, C.V. Hampton, and Wm.C. McHarris

As a continuation of the study of light Praseodymium nuclei [1], Interacting Boson Approximation (IBA) calculations were performed on the even-even Ce "cores" of the odd mass Pr nuclides with masses between A=128 and A=136. Interacting Boson Fermion Approximation (IBFA) calculations were performed on the odd-mass ^{131}Pr and ^{133}Pr nuclides.

IBA is a group theoretical model which utilizes the symmetries of a "boson" structure description of the nucleus. Even-even nuclides are composed of sets of s-bosons and d-bosons which, in the case of the IBA-1 model, are treated as indistinguishable for specific proton and neutron identities. The mathematical representation of the Hamiltonian is given by the expression:

$$H = n_d\varepsilon_d + \kappa'' P\cdot P + \kappa' L\cdot L + \kappa Q\cdot Q.$$

Where n_d is the number of d-bosons in the system, ε_d is the effective occupation of that boson number, P is the pairing interaction (for the sake of simplicity constrained to 0 in these calculations), L is the dipole interaction, and Q is the quadrupole interaction. Odd mass systems are based on the core structure of s-d bosons with the addition of an Hamiltonian for the odd particle (fermion) in the system and an interaction potential between the fermion and the even-even core. This can be expressed as:

$$H = H_{IBAcore} + H_{fermion} + V_{boson-fermion}.$$

The calculations for the even-even nuclides were performed with the code PHINT [2]. Table 1 shows the "best-fit" values of the parameters determined by a series of calculations for the Ce core nuclides.

Table 1: Parameters for PHINT program calculations of even-even Ce core nuclides in the light Pr region.

Parameter/Nuclide	^{128}Ce	^{130}Ce	^{132}Ce	^{134}Ce	^{136}Ce
No. Bosons	10	9	8	7	6
EPS	0.42	0.44	0.46	0.50	0.55
QQ	-0.025	-0.025	-0.025	-0.025	-0.025
CHQ	-2.50	-2.50	-2.95	-2.95	-2.95
ELL	0.022	0.022	0.028	0.030	0.040

Figure 1 shows a comparison of the experimentally observed energies in the Ce nuclides with those calculated in the IBA model. The calculated rotational levels are in remarkably good agreement up to 3 MeV. This consistency is achieved, in part, by varying in a systematic fashion three of the input parameters in the calculations. The relatively large value of the dipole interaction term is significant in interpretations of general structures of these nuclides. It has been demonstrated in the Rhenium region, that prolate spheroidal shapes can be fit with relatively minor contributions from the dipole term.[4] The nuclides in the light rare earth region can be considered as less pure in their quadrupole deformation character.

Table 2 displays the parameters for the negative parity bands in the odd mass nuclide calculations. The code ODDA,[3] was used with multipole expansion parameters, explicit orbital occupation probabilities

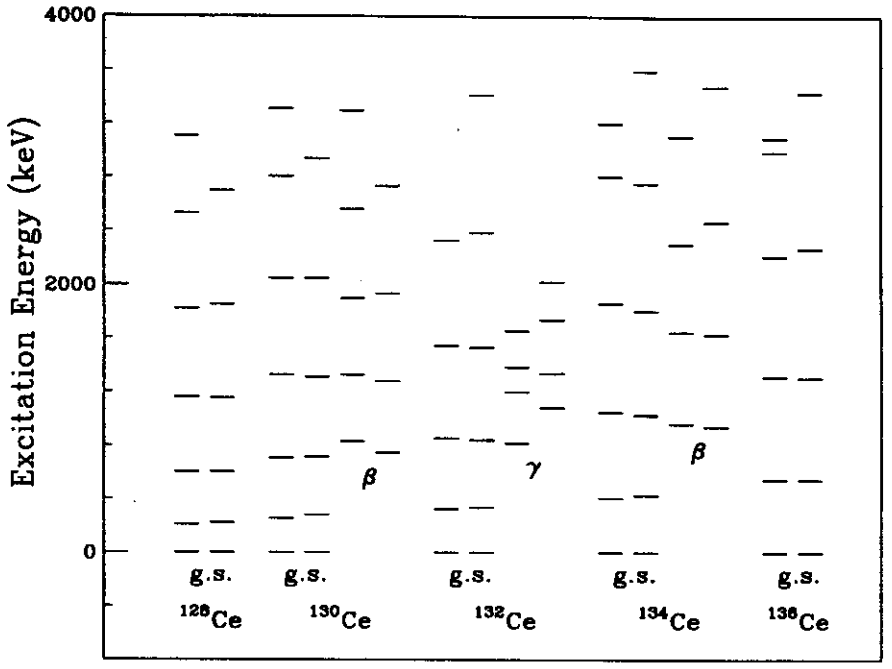

Figure 1: Comparison of experimentally observed energies and theoretical energies calculated in the IBA model for Ce core nuclides. The nucleus and band identification is noted at the bottom, g.s. - ground state and β or γ for excited bands. Experimental level is on the left and calculated level is on the right of each pair of hashes.

and single particle energies. Specifically, the additional non-fixed parameters which are required are the boson-fermion interaction strengths: BFQ – quadrupole, BFE – exchange and BFM – monopole. As with the case of their even-even cores, the calculated levels of the ground bands show very good agreement with the experimentally observed levels. And again, as in the case of the even-even cores, the quadrupole strengths are much smaller than one would expect from "good" rotors with significant quadrupole deformations.

Table 2: Parameters for ODDA program calculations of ^{131}Pr and ^{133}Pr.

Nuclide/Parameter	Core	CHI	BFQ	BFE	BFM	VSQ	PEN
^{131}Pr	^{130}Ce	-1.32	0.08	1.20	-0.10	0.898,0.067	0.00, 4.35
^{133}Pr	^{132}Ce	-1.32	0.08	1.20	-0.10	0.898,0.067	0.00, 4.35

A comparison of experimental and theoretical excitation energies of the ^{131}Pr and ^{133}Pr negative parity bands look very similar to Fig. 1. Deviations of the calculated levels from the observed are less than 10% with the exception of the bandhead or first member of the rotational band.

Further IBA calculations are in progress for light rare-earth nuclides including other even-even, odd mass, and some interpolative calculations for odd-odd nuclides. A more complete data set will enhance the understanding of the dipole-quadrupole interactions within the IBA in this region.

References

1. W.A. Olivier, C.V. Hampton, and Wm.C. McHarris, NSCL Annual Report, 142 (1995).
2. O. Scholten, Program package PHINT (1984).
3. O. Scholten, Program package ODDA (1985).
4. W.-T. Chou, PhD. Thesis, MSU (1989).